Contributions to Mineralogy and Petrology (2022) 177: 73
https://doi.org/10.1007/s00410-022-01940-7

ORIGINAL PAPER

The high-K calc-alkaline to shoshonitic volcanism of Limnos, Greece: implications for the geodynamic evolution of the northern Aegean

Leon Gläser[1] · Anna Grosche[1] · Panagiotis C. Voudouris[2] · Karsten M. Haase[1]

Received: 23 March 2022 / Accepted: 10 July 2022 / Published online: 21 July 2022

Abstract

Genetic models for the formation of K-rich magmas in subduction-related settings range from partial melting of subduction-affected mantle sources to melting of crustal rocks depending on the local tectonic framework. The Miocene high-K calc-alkaline to shoshonitic rocks of Limnos Island reflect the magmatic activity in the northern Aegean, which migrated southwards in response to trench retreat and the collision of continental terranes in the Hellenic subduction system. New whole rock and mineral data of basaltic andesites, dacites and monzonites from Limnos indicate that the magmas underwent fractional crystallization of olivine, clinopyroxene, amphibole, apatite, and Fe-Ti oxides at 1100 to 700 °C and 0.5 to 0.1 GPa without significant assimilation of crustal rocks during the magma evolution. The strong enrichment of large ion lithophile elements and light rare-earth elements relative to depleted heavy rare earth and high-field strength elements points towards a mantle source that has been extensively hybridized by subducted sedimentary material. New Sr–Nd-Pb isotope data reveal a distinct isotopic composition of the Limnos rocks with high $^{207}Pb/^{204}Pb$ at low $^{206}Pb/^{204}Pb$ and $^{143}Nd/^{144}Nd$ ratios that is likely related to the subduction of the continental crustal succession of the Apulian block which was subducted prior to the onset of magmatism on Limnos. Partial melting models assuming a hybridized mantle source suggest that the primary melts of Limnos formed by melting of a phlogopite pyroxenite at melting degrees of 5 to 10%. Compositional differences between high-K calc-alkaline and shoshonitic magmas are explained by variable melting degrees and varying amounts of sediment supply to the mantle. The magmatic and tectonic evolution of Limnos island is typical for the Oligocene and Miocene volcanic centres of the migrating western Aegean arc front.

Keywords Radiogenic isotopes · Subduction · Partial melting · Petrogenesis · Shoshonite · Trace element

Introduction

Magmas with highly variable compositions form along the Earth's subduction zones reflecting complex processes in the upper mantle of mixing mantle and crustal rocks, of element transport by hydrous material and of partial melting (Miyashiro 1974; McCulloch and Gamble 1991; Hawkesworth et al. 1993). Additionally, the composition of the magmas is frequently altered during the ascent through the lithosphere, particularly by reaction with the rocks of the continental crust (e.g. Davidson et al. 2005). Thus, many volcanic rocks along continental subduction zones are andesitic to rhyolitic yielding little evidence for primary mafic magmas from the mantle in their genesis. There is general consensus that most primary magmas at subduction zones are basaltic and form in the asthenospheric mantle wedge by hydrous melting with variable involvement of decompression melting (Kushiro 2007; Schmidt and Jagoutz 2017). Potassium-rich magmas are frequent in both continental and oceanic subduction zones, and magmas in many arcs range from medium- to high-K calc-alkaline to shoshonitic compositions (Wheller et al. 1987; Robert et al. 1992; Sun and Stern 2001). For example, the K-rich magmas in oceanic island arcs like the Marianas or the Sunda-Banda arcs are generally believed to form from the mantle wedge mainly reflecting the addition

Communicated by Timothy L. Grove.

✉ Leon Gläser
GlaeserLeon@gmx.de

[1] GeoZentrum Nordbayern, Friedrich-Alexander-Universität (FAU) Erlangen-Nürnberg, Schlossgarten 5, 91054 Erlangen, Germany

[2] Faculty of Geology and Geoenvironment, National and Kapodistrian University of Athens, 15784 Athens, Greece

of fluids and partial melts from subducted sediments, continental crust and basaltic crust (e.g. Sun and Stern 2001; Elburg et al. 2004). Other models suggest the formation of K-rich magmas in continental arcs by melting of sediment diapirs or mélanges of sediment with hydrated peridotite in the hot region of the mantle wedge (Behn et al. 2011; Marschall and Schumacher 2012). Primitive magmas in some arcs have high-Mg andesitic compositions which could represent melts from mantle peridotite with high water content or mixtures of peridotite with sedimentary material (Kelemen 1995; Straub et al. 2008). Additionally, many K-rich magmas seem to form after subduction ceased and are thus believed to be 'post-collisional' due to melting of metasomatized lithospheric mantle or lower crustal rocks (e.g. Sekine and Wyllie 1983; Foley 1992; Condamine and Médard 2014). However, lithospheric mantle of the upper plate that is not part of the convecting mantle wedge has temperatures < 1100 °C (Perrin et al. 2018). Partial melting of peridotite with such low temperature requires either massive addition of volatiles or the re-heating by hot mantle material, for example, following extension and rifting of the lithosphere causing an ascent of hot asthenosphere.

The formation of Cenozoic magmas in the Aegean is closely related to the complex tectonic history with alternating periods of ocean subduction and collision/subduction of continental fragments from Eocene to present (Menant et al. 2016; Schaarschmidt et al. 2021a). The occurrence of widespread high-K to shoshonitic magmatism during upper Miocene makes it a suitable area to study the origin of K-rich magmas in subduction-related settings. Here, we provide new petrological and geochemical data on the high-K calc-alkaline to shoshonitic volcanic and plutonic rocks from Limnos island that were interpreted to have formed either during or after subduction. The data are used to assess the influence of fractional crystallization and crustal contamination during the magma evolution. We use trace element and new Sr–Nd–Pb isotope data to determine the source components of the primary melts and to develop a quantitative partial melting model for different mantle lithologies that can be applied to the genesis of K-rich magmas elsewhere.

Geological setting

Regional tectonic background

The Aegean subduction zone migrated southwards in the past 30 million years due to slab-rollback, that caused extension in the back-arc and arc region (Jolivet and Brun 2010). The Aegean Sea lies within a complex succession of thrusted terranes that have undergone periods of alternating stress regimes as a result of the ongoing convergence between Africa and Eurasia (Fig. 1a). During the Upper Cretaceous to Eocene, the north-eastward drifting continental blocks of Pelagonia and Apulia collided with Rhodopia and Serbo-Macedonia, which led to the amalgamation with Eurasia (Kydonakis et al. 2015). Its boundaries are marked by two suture zones that formed after the closure of two Neo-Tethyan ocean branches surrounding Pelagonia. The Vardar-Suture-Zone between Pelagonia and the Serbo-Macedonian Massif crosses the Aegean Sea south of Limnos and is most likely linked to the Izmir-Ankara Suture (Çelik et al. 2011). The almost parallel running Pindos suture zone extends southeast of the Dinarides into the South Aegean Sea and separates Apulia to the west from Pelagonia to the east (Fig. 1a). However, the exact locations and correlations of these suture zones are still debated (Marroni et al. 2014; Taymaz et al. 2007).

Widespread extension is believed to have commenced in the Rhodope massif in middle Eocene time and from then on progressed southwestwards (Brun et al. 2016). The extension was caused by the southward retreat of the Hellenic trench as a result of slab-rollback, induced by the subduction and accretion of continental blocks (Faccenna and Brun 2008). Paleomagnetic data revealed that the extension followed a clockwise rotation of the continental blocks opening the Aegean Sea (Brun and Sokoutis 2010; van Hinsbergen et al. 2005). Additionally, post-orogenic collapse and crust-mantle delamination may have played a role in the formation of the extensional structures, such as metamorphic core-complexes and sedimentary basins, that can be observed in the Aegean (Brun et al. 2016; Kydonakis et al. 2015). Slab retreat was accompanied by systematic southward migration of magmatic activity in the western Aegean (e.g. Jolivet et al. 2015) which was suggested to reflect consecutive ascent of mélange diapirs from the slab top (Schaarschmidt et al. 2021a). Alternatively, lithospheric delamination or slab detachment may have been the cause for melt generation causing, for example, calc-alkaline and shoshonitic volcanism in western Anatolia (e.g. Aldanmaz et al. 2000). The early to middle Miocene age of the western Anatolian volcanism correlates with the volcanic activity of Limnos, which could suggest a similar origin. Thus, Pe-Piper et al. (2009) proposed that upwelling of the asthenosphere beneath Limnos was a result of slab breakoff and mantle-derived magmas caused partial melting of the lower crust followed by mixing of the different melts. During the upper Miocene the NE-SW extension was further aided by dextral movements along large-scale strike-slip faults, such as the North Anatolian Fault Zone (NAFZ, Fig. 1a) (Armijo et al. 1999; Brun et al. 2016). The crustal thickness beneath the northern Aegean Sea is estimated at 25 to 30 km, but may have been up to 50 km thick prior to the two-stage back-arc extension in the Oligocene/Miocene and again in the Plio-/Pleistocene (Tirel et al. 2004; Sodoudi et al. 2006; Karabulut et al. 2019). Tirel et al. (2004) point out that the

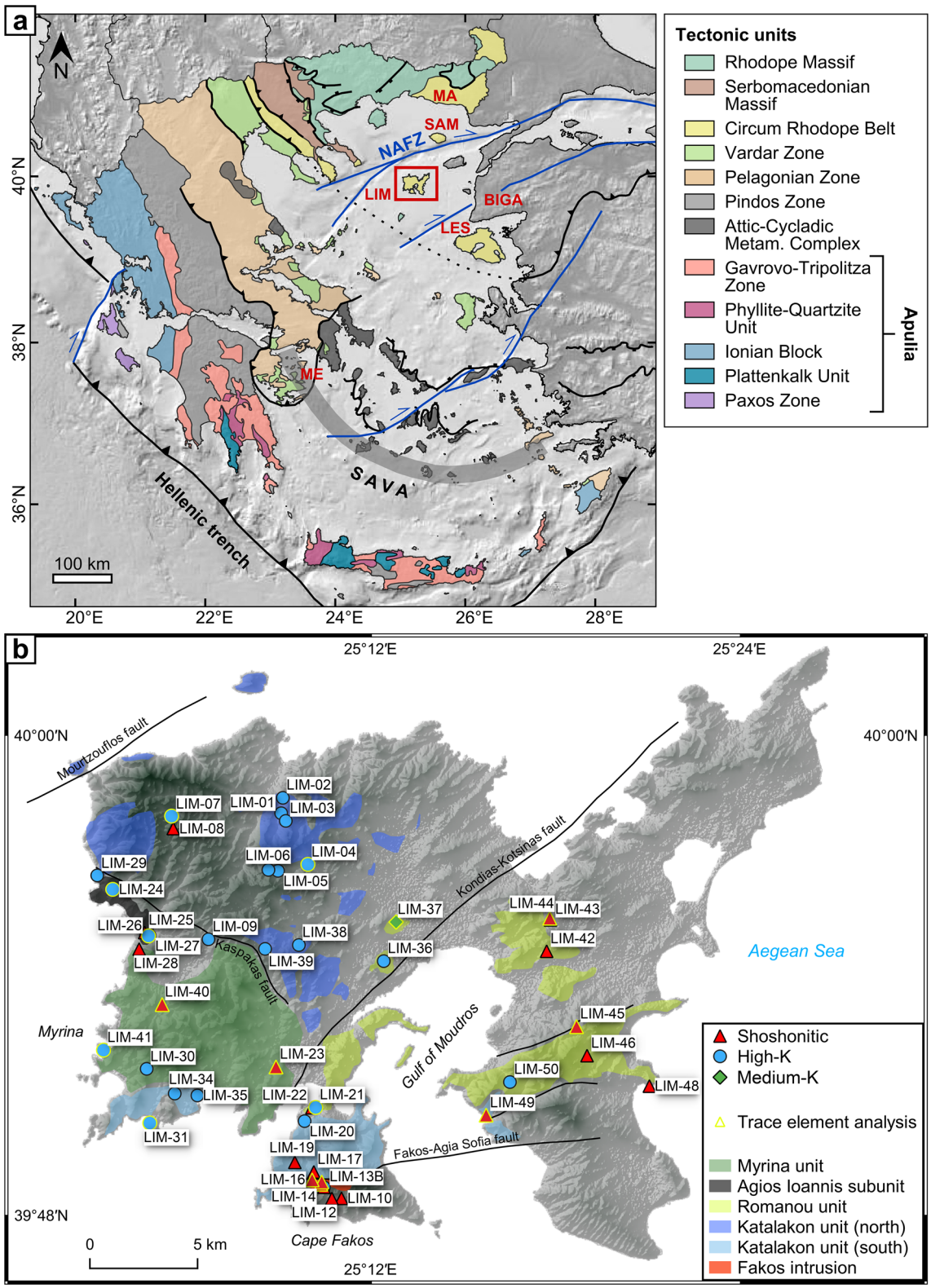

Fig. 1 (**a**) Map of the Aegean Sea depicting the main tectonic units of Greece and western Turkey. (**b**) Simplified map of Limnos with sample locations. Samples used for trace element and Sr–Nd–Pb isotope analysis are marked with yellow rims. Extent of the volcanic units according to Innocenti et al. (1994) and Pe-Piper et al. (2009) and locations of faults according to Pavlides et al. (2009)

crust of the Aegean Sea shows a flat Moho similar to the Basin and Range probably reflecting lower crustal flow.

Geology of Limnos

The island of Limnos covers an area of ~ 400 km^2 in the northern Aegean Sea, southwest of the island of Samothraki (Fig. 1a). Limnos lies in the Thrace Basin and consists of sedimentary and volcanic rocks forming a rugged morphology in the west, whereas the eastern portion of Limnos is low with a smooth morphology (Fig. 1b). These two parts of the islands are divided by the Kondias–Kotsinas fault zone consisting of a series of NE–SW striking right-lateral strike-slip faults that may have also affected the emplacement of magmatic intrusions (Koukouvelas and Aydin 2002; Pavlides et al. 2009). The sediments are mainly sand- and siltstones with ages from Middle Eocene to Lower Miocene representing deep-marine turbidite deposits with occasional tuff layers overlain by continental conglomerates, marls, and mudrocks (Innocenti et al. 1994; Caracciolo et al. 2011). The continental sediments are overlain and intruded by lava flows and domes, subvolcanic rocks, ignimbrites, and volcaniclastic deposits. The oldest rocks of the basement comprise a succession of Middle Eocene to Early Oligocene flysch deposits representing a submarine fan in the fore-arc basin of the migrating subduction zone (Maravelis et al. 2016). From the Late Oligocene to the Middle Miocene three N–S-directed compressional tectonic phases occurred during the deposition of the overlying sedimentary units causing folding of the topmost strata and the development of tensional structures (Tranos 2009). This compression affected the subduction dynamics and was probably due to the collision of the Apulian block with the Eurasian Plate which led to uplift, erosion of the folds, and a transition from marine to continental sediments prior to the onset of Early Miocene volcanism on Limnos (Erbil et al. 2021; Innocenti et al. 1994; Tranos 2009). Tectonic reconstructions of the Aegean subduction zone suggest that the Apulian continental block had been accreted and partially subducted by ~ 23 Ma, which was followed by subduction of oceanic lithosphere of the eastern Mediterranean (Ring et al. 2010; Jolivet et al. 2013). Metasedimentary rocks of the lowest tectonic unit of the Cyclades, the Basal Unit, show the peak of high-pressure metamorphism with 0.8 to 1.0 GPa and 350 to 400 °C and ages of 24 to 21 Ma indicating the subduction of thick layers of clastic and carbonate sediments in the Early Miocene (Ring et al. 2001).

Three major volcanic rock units were suggested to occur on Limnos island (Fig. 1b) in addition to a small-scale monzonite intrusion at Cape Fakos; the effusive Katalakon unit, the pyroclastic Romanou unit, and the Myrina unit consisting of the youngest lava domes and occasional flows (Innocenti et al. 1994). Potassium-Ar ages of the Limnos volcanic rocks indicate ages of 21 to 18 Ma (Innocenti et al. 1994; Pe-Piper et al. 2009). The oldest volcanic products on Limnos belong to the southern Katalakon unit (Fig. 1b), which consists of altered andesitic and dacitic lava domes and hosts the monzonitic intrusion at Cape Fakos. Towards the east, around the Gulf of Moudros, the Katalakon unit is overlain by pyroclastic deposits, dacites, and latites of the Romanou unit, which show the highest potassium contents. Based on age dates, Pe-Piper et al. (2009) suggested that the Romanou unit is older than the northern Katalakon unit. The Myrina unit is located in southwest Limnos, and separated from the northern Katalakon unit by the NW–SE striking Kaspakas fault (Pavlides et al. 2009). It comprises the island's youngest volcanic domes and lava flows with mainly dacitic compositions. The northern lavas along the coastline have been assigned to the Agios Ioannis subunit by Pe-Piper et al. (2009) due to their transitional compositions in relation to lavas of the two neighbouring Myrina and Katalakon units (Fig. 1b). Whereas Innocenti et al. (2009) suggested an origin of the magmas in the mantle above a subducting slab, Pe-Piper et al. (2009) proposed that the Limnos lavas represent mixtures of a mantle-derived basanitic melt and a partial melt of amphibolite in the lower crust.

Sampling and analytical methods

Sampling and sample preparation

For this study, 50 magmatic rock samples were collected and studied at the GeoZentrum Nordbayern (Friedrich-Alexander Universität Erlangen-Nürnberg) with a focus on the geochemical whole rock major and trace element as well as radiogenic isotope composition. The samples mostly consist of lavas from domes and flows as well as from dykes. According to the geological map after Innocenti et al. (1994), the samples represent the three major volcano-stratigraphic units and are distributed over the entire island (Fig. 1b). In addition, three monzonite samples from the southern Fakos intrusion were examined.

Analysis of mineral compositions

Polished thin sections of ten samples of both shoshonitic and high-K rocks from variable locations were petrographically examined and the minerals were analysed using the JEOL JXA-8200 Electron Probe Microanalyser at the GeoZentrum Nordbayern (GZN). For the measurement of core and rim compositions of plagioclase, amphibole and clinopyroxene an electron beam of 3 µm diameter with a current of 15 nA and an acceleration voltage of 15 kV was used. Magnetite and ilmenite grains were analysed using a 1 µm beam with a beam current of 20 nA and an acceleration voltage

of 20 kV. The counting times and detection limits of the analysed elements are listed in Schaarschmidt et al. (2021b) and the results of all mineral analyses can be found in the electronic supplement of this work (Table S1). The mineral compositions were used to estimate the pressure–temperature conditions and the volatile content of the magmas during crystallization by applying different thermobarometric models (Table 1).

Whole rock geochemistry

Sample blocks of fresh rock material were ultrasonically cleaned in deionized water and dried for 24 h in a drying oven at 60 °C. After crushing of the blocks by a hydraulic press, an agate mill was used to pulverize the samples to grain sizes below 40 µm. The powder was dried for 24 h at 100 °C.

The contents of the major elements (> 0.1 wt.%) were determined by X-ray fluorescence (XRF) using an energy dispersive Spectro Xepos He X-ray fluorescence spectrometer at GZN. Samples were homogenized to melt discs using lithium-tetraborate ($Li_2B_4O_7$). Loss on ignition (LOI) was calculated by determining the weight difference of each sample before and after the ignition in a muffle furnace. Accuracy and precision of the measurements were determined by multiple measurements of the international rock standards BR and BE-N for basalts and GA and AC-E for granites (Govindaraju 1994; electronic supplement Table S1). Repeated analyses of the standards BR and BE-N gave an accuracy better than 9% for P_2O_5, better than 6% for Na_2O and better than 3% for the remaining major elements. The precision of the analysis, expressed as the relative standard deviation (RSD, 2 s), was better than 3% for Na_2O, better than 2% for MgO and P_2O_5, and better than 1% for all other major elements. For the granite standards GA and AC-E, the accuracy was better than 7% for Fe_2O_3 and better than 5% for all other major elements, except for MgO and P_2O_5, which have too low absolute MgO and P_2O_5 contents in the felsic standard material. The relative precision (2 s) was better than 1% for all major elements save MgO (12%) and P_2O_5 (6%).

Sixteen samples were selected for trace element analyses based on their locations and their major element contents to cover a preferably wide range in SiO_2 and K_2O. A detailed description of the preparation procedure is given in Schaarschmidt et al. (2021b) and is briefly described here. The trace element concentrations were determined on a Thermo-Fischer X-Series 2 Q-ICP-MS at GZN together with multiple measurements of the basalt standard BHVO-2 (GeoReM; Jochum et al. 2016). All trace elements had an accuracy better than 9% except for Zn (< 17%), Sb (< 46%), Cs (< 28%) and the long-term reproducibility of 2020 (2 s; $n = 30$) was better than 14% for all trace elements excluding Ni and Cu (< 20%) and Cs (< 40%) (electronic supplement Table S1). Due to the partial dissolution of zircon during digestion of rock powder, the Zr concentration determined by XRF

Table 1 Temperature, pressure, water content and oxygen fugacity calculations based on different models for amphibole (amph), hornblende (hbl), clinopyroxene (cpx), magnetite/ilmenite (mt/ilm) and plagioclase (plg) compositions. The results are the average values of the number (n) of analysed crystals. Values in brackets are from enclaves. Pressure and temperature estimates of all mineral analyses are visualized in Fig. 1

		High-K samples			Monzonite	Shoshonitic samples	
		LIM-03	LIM-32	LIM-37	LIM-14	LIM-25	LIM-42
Andersen and Lindsley (1985), Lepage (2003), Powell and Powell (1977), Spencer and Lindsley (1981)	$T_{mt/ilm}$ [°C]	860	–	–	–	890	730
	fO_2	−11	–	–	–	−11	−14
	n	3	–	–	–	4	4
Mutch et al. (2016)	$P_{Al\ in\ hbl}$ [GPa]	–	0.53	0.34 (0.43)	0.10	–	–
	n	–	6	5	10	–	–
Putirka et al. (2003)	$T_{cpx\ [°C]}$	–	–	–	1052	–	1126 (1136)
	P_{cpx} [GPa]	–	–	–	0.24	–	0.52 (0.64)
	n	–	–	–	5	–	10
Ridolfi et al. (2010)	T_{amph} [°C]	–	960 ± 20	890 ± 20	760 ± 20	–	–
	P_{amph} [GPa]	–	0.35 ± 0.04	0.21 ± 0.02	0.04 ± 0.01	–	–
	fO_2	–	−9.9 ± 0.4	−10.9 ± 0.4	−12.0 ± 0.4	–	–
	H_2O [wt.%]	–	4.6 ± 0.7	4.4 ± 0.5	2.4 ± 0.4	–	–
	n	–	19	10	22	–	–
Waters and Lange (2015)	H_2O [wt.%]	5.3 ± 0.1	4.3 ± 0.1	6.7 ± 0.1	–	4.0 ± 0.1	4.8 ± 0.1
	n	15	20	8	14	18	12

analysis was considered for all interpretations and diagrams.

For Sr, Nd, and Pb isotope analysis 100–150 mg of rock powder was dissolved and processed following the procedure described in Schaarschmidt et al. (2021b). Lead, Sr and Nd was separated from the rock matrix using different ion exchange columns (Schaarschmidt et al. 2021b). Isotope measurements of Sr and Nd were carried out on a Thermo-Fischer Triton TIMS (thermal ionization mass spectrometer) at GZN. Strontium isotope measurements were corrected for instrumental mass fractionation assuming $^{88}Sr/^{86}Sr = 0.1194$ and corrected for the contribution of ^{87}Rb to mass 87. Neodymium isotope data were corrected for mass fractionation using a $^{146}Nd/^{144}Nd$ ratio of 0.7219. Samarium interference on masses 144, 148, 150 was corrected by measuring ^{147}Sm. The Sr isotopic ratios have a maximum internal uncertainty of ± 0.000008 (2 s) and were normalized to the NBS987 standard with $^{87}Sr/^{86}Sr = 0.710250$ and an average measured value of 0.710276 ± 0.000011 (2 s, $n = 3$). Likewise, the Nd isotopic ratios (2 s = ± 0.000005) were normalized to the Erlangen Nd standard with $^{143}Nd/^{144}Nd = 0.511541$ and an average value yielding 0.511538 ± 0.000010 (2 s, $n = 4$). Lead isotope measurements were carried out on a Thermo Fisher Neptune multi-collector ICP-MS at GZN using a $^{207}Pb/^{204}Pb$ double spike to correct for instrumental mass fractionation. The Pb fraction was diluted with 2% HNO_3 to a concentration of approximately 20 ppb. One part of this solution was spiked in order to obtain a $^{208}Pb/^{204}Pb$ ratio of about 1. The double spike, with a $^{207}Pb/^{204}Pb$ ratio of 0.5, was calibrated against a solution of the NBS982 equal atom Pb standard. Spiked and unspiked sample solutions were introduced into the plasma via a Cetac Aridus desolvating nebulizer, and measured in static mode. Interference of ^{204}Hg on mass 204 was corrected by monitoring ^{202}Hg. An exponential fractionation correction was applied offline using the iterative method of Compston and Oversby (1969). The correction was typically 4.5‰ per amu. The typical uncertainties of individual analyses are ± 0.0003, ± 0.0003 and ± 0.0007 for $^{206}Pb/^{204}Pb$, $^{207}Pb/^{204}Pb$ and $^{208}Pb/^{204}Pb$, respectively. The isotopic ratios were normalized to the NBS981 standard with $^{206}Pb/^{204}Pb = 16.9410$, $^{207}Pb/^{204}Pb = 15.4993$, and $^{208}Pb/^{204}Pb = 36.7244$. Repeated measurements of the NBS981 Pb isotope standard gave average $^{206}Pb/^{204}Pb$, $^{207}Pb/^{204}Pb$, $^{208}Pb/^{204}Pb$ ratios of 16.9405 ± 0.0018, 15.4979 ± 0.0010 and 36.7190 ± 0.0032, respectively (2 s). The initial isotope ratios of Sr, Nd and Pb were calculated for each sample by assuming an emplacement age of 20 Ma. The results of whole rock major element, trace element and Sr–Nd-Pb isotope analyses can be found in the electronic supplement (Table S2).

Results

Petrography

The Limnos lavas and the monzonite are characterized by a fine- to medium-grained porphyritic texture with a holo- to hypocrystalline groundmass surrounding phenocrysts of plagioclase, quartz, amphibole, biotite and clinopyroxene. The colour of the groundmass varies between greenish light grey to dark brown. Some samples exhibit orientated phenocrysts (LIM-14, LIM-21, LIM-25). Plagioclase is the dominant phase in all samples and mostly has a euhedral to subhedral shape and frequently shows a zonation. Quartz is more abundant in samples of the Katalakon unit, whereas clinopyroxene phenocrysts only occur in rocks of the Romanou unit and the Fakos monzonite. The clinopyroxenes are of light brown to green colour and rarely show growth zoning. The samples contain accessory apatite, zircon, magnetite, ilmenite and titanite. The Fakos monzonite (LIM-14) further contains euhedral orientated K-feldspar phenocrysts. Lavas from Katalakon south and Romanou host enclaves of several cm size with a similar mineralogy, but smaller phenocryst size. Most samples went through minor degrees of hydrothermal alteration resulting in partial chloritization of pyroxene and sericitization of feldspar. Vesicles occur in several samples and are filled with calcite.

Mineral composition

Plagioclase is the most abundant mineral in all rocks from Limnos. The An content ranges from a maximum value of 54 (LIM-03) to the lowest value of 21 (LIM-14) with the majority of crystals with An contents between 30 and 50 (andesine). Plagioclase of one shoshonitic sample (LIM-42) is considerably more potassic (Or content 4 to 9) than crystals of the other samples. Within single plagioclase crystals, the An content decreases from the cores toward the rims in all samples and profiles across individual grains show normal zoning patterns (LIM-03, LIM-37, LIM-42) but also few irregularly zoned grains with more sodic cores in LIM-14. The An contents and the whole rock compositions of each sample were used for the plagioclase-liquid hygrometer by Waters and Lange (2015) to calculate the water content of the melt, ranging from 4.0 to 4.8 wt.% in shoshonitic samples and from 4.3 to 6.7 wt.% in high-K samples (Table 1).

Amphibole in samples LIM-14 and LIM-37 largely classifies as Mg-hornblende besides some crystals of tschermakitic compositions with higher Mg and Si contents in

sample LIM-37 (Leake et al. 1997). The thermobarometric model by Ridolfi et al. (2010) was applied to calculate the temperature, pressure, water content and oxygen fugacity of the samples (Table 1). The amphiboles yield crystallization conditions of 0.15 to 0.40 GPa at 900 to 960 °C for the high-K lavas and ~ 0.04 GPa at 760 °C for the monzonite (Fig. 2, Table 1). The calculated water contents differ slightly compared to the results of the plagioclase hygrometer, but also record the lowest H_2O contents for the monzonite (Table 1). The calculated oxygen fugacity log fO_2 ranges from -12 (LIM-14) to -10 (LIM-32), which corresponds to a ΔFMQ of + 2 (relative to the fayalite-magnetite-quartz buffer). The geobarometer of Mutch et al. (2016) for granitic rocks depends only on the Al content of the amphiboles and yields slightly higher pressures for all three samples (Table 1).

Clinopyroxene occurring in two analysed samples (LIM-14 and LIM-42) has diopside-augite compositions with the monzonite (LIM-14) clinopyroxenes having slightly higher Ca contents. In the lack of glass analysis, the whole rock compositions of the samples were used for the clinopyroxene-liquid thermobarometer by Putirka et al. (2003). Clinopyroxene records crystallization temperatures around 1052 °C and 1130 °C and pressures of 0.24 GPa and 0.52 GPa for the monzonite (LIM-14) and the shoshonitic lava (LIM-42), respectively (Fig. 2, Table 1).

Magnetite–ilmenite pairs were used to estimate the crystallization temperature and the oxygen fugacity of the magmas. Based on their Fe content and V/Ti ratio only magmatic and no re-equilibrated magnetites were taken into account (Wen et al. 2017). The remaining mineral pairs provide approximations of the temperature and oxygen fugacity, which correspond to FMQ + 2 at 730 to 890 °C for the shoshonitic and high-K lavas. The values overlap with previous data from Methana (Schönhofen et al. 2020) and Nisyros (Seymour and Lalonde 1991) at the SAVA, but are higher than the values observed at Santorini (FMQ to FMQ + 1; Fabbro et al. 2013).

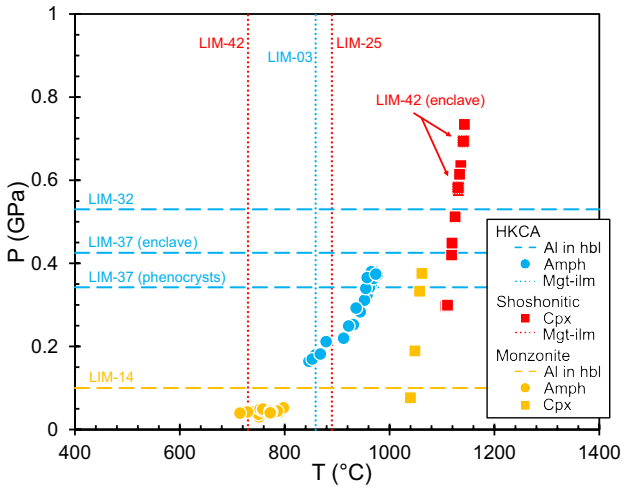

Fig. 2 Results of the geothermobarometry calculations for high-K calc alkaline (HKCA), shoshonitic and monzonite samples. Al in hbl: Al-in-hornblende barometer after Mutch et al. (2016). Amph: amphibole thermobarometer after Ridolfi et al. (2010). Cpx: clinopyroxene thermobarometer after Putirka et al. (2003). Mgt-ilm: thermometer for magnetite–ilmenite pairs after Andersen and Lindsley (1985), Lepage (2003), Powell and Powell (1977) and Spencer and Lindsley (1981)

Major element composition

The SiO_2 contents of the Limnos samples range between 55 and 65 wt.%, i.e. between basaltic andesites and dacites, overlapping with data from previous studies (Innocenti et al. 1994; Pe-Piper et al. 2009). About half of the samples can be classified as high-K rocks with the other half belonging to the shoshonitic series (Fig. 3a, Peccerillo and Taylor 1976). All high-K samples follow the calc-alkaline trend of decreasing FeO_T and MgO contents and increasing alkali contents with increasing SiO_2 (Fig. 3). The samples have LOI values between 1 and 7 wt.% indicating variable amounts of hydrous minerals and possibly carbonate alteration. For example, the dike sample LIM-07 is propylitized suggesting late hydrothermal alteration. However, most of the samples contain hydrous magmatic minerals biotite and amphibole that can probably account for up to 3 wt.% LOI. The lavas generally follow continuous major element trends of increasing K_2O and decreasing CaO contents with increasing silica (Fig. 3) whereas alteration should cause less systematic variation. Thus, we conclude that the major element composition of samples with LOI < 3 wt.% is not significantly altered, with the possible exception of some samples with anomalous K_2O, CaO, Al_2O_3 or Na_2O contents (LIM-07, LIM-10, LIM-16, LIM-19, LIM-25, LIM-37, LIM-45). However, even samples with high LOI do not show anomalous Sr–Nd-Pb isotopic ratios supporting the reliability of the data.

The rocks of the southern Katalakon unit, the adjacent Fakos monzonite and the Romanou unit mainly belong to the shoshonitic series, whereas the Katalakon north and Myrina units follow the high-K trend. Based on the published age record, this suggests a general evolution from shoshonitic to high-K calc-alkaline magmatism with time (Innocenti et al. 1994; Pe-Piper et al 2009). The major element variations of the Limnos magma series (Fig. 3) are compared to published data from Limnos (Pe-Piper et al. 2009; Fornadel et al. 2012) and similar magmatic rocks from the neighbouring islands Lesbos and Samothraki (Pe-Piper and Piper 1992; Pe-Piper et al. 2014; Vlahou et al. 2006) and the South Aegean Volcanic Arc (SAVA; Bailey et al. 2009; Büttner et al. 2005; Elburg et al. 2014, 2018; Elburg and Smet 2020; Fabbro et al.

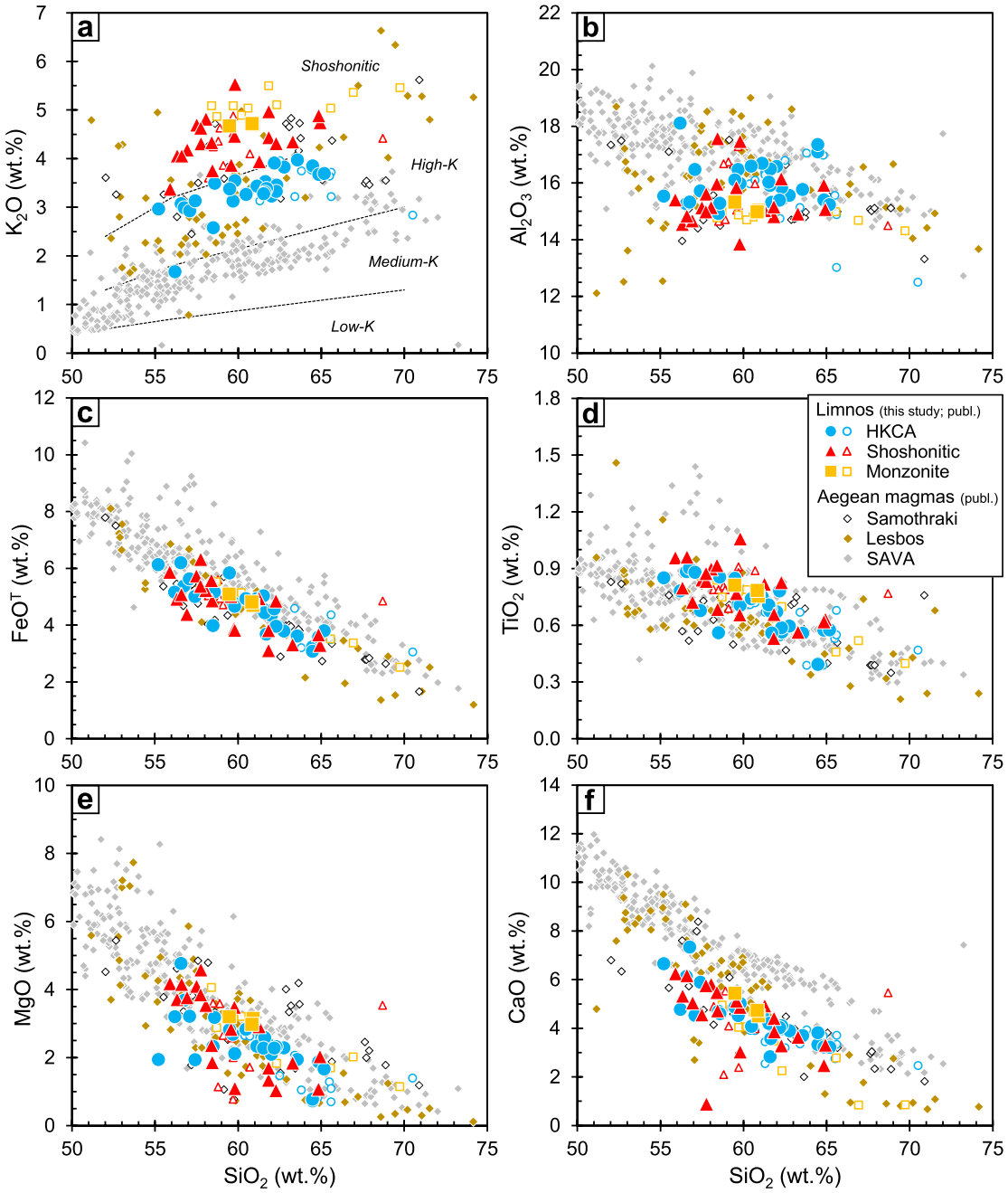

Fig. 3 (**a**) Silica vs. K_2O diagram with the classification of the magmatic series after Peccerillo and Taylor (1976). (**b**–**f**) Silica content vs. major elements (as analysed). Samples of this work are plotted alongside previously published data of rocks from Limnos (Pe-Piper et al. 2009), Samothraki (Vlahou et al. 2006), Lesbos (Pe-Piper and Piper 1992; Pe-Piper et al. 2014) and the South Aegean volcanic arc (SAVA; Bailey et al. 2009; Büttner et al. 2005; Elburg et al. 2014, 2018; Elburg and Smet 2020; Fabbro et al. 2013; Innocenti et al. 1981; Kirchenbaur et al. 2012; Nicholls 1971; Pe-Piper and Piper 1994)

2013; Innocenti et al. 1981; Kirchenbaur et al. 2012; Nicholls 1971; Pe-Piper and Piper 1994). Overall, our results are consistent with the data of previous studies, but cover a larger range of SiO_2 especially at low SiO_2 contents. Magmas from Lesbos and Samothraki have a larger range of SiO_2 (50 to 72 wt.%) than rocks from Limnos, but follow the same trends. The shoshonitic rocks and monzonites exhibit slightly lower Al_2O_3 and higher P_2O_5 contents than the high-K calc-alkaline samples, while all other major element contents show no major differences between the two series.

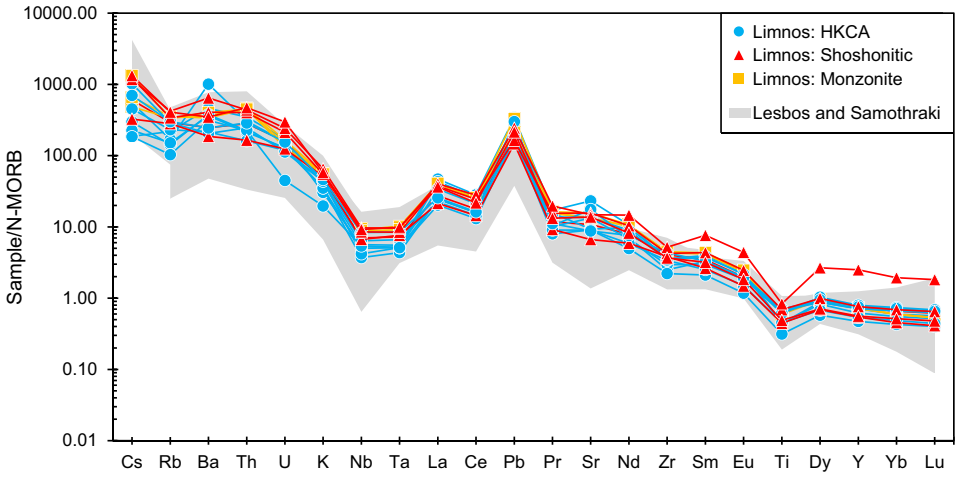

Fig. 4 Multi-element diagram normalized to MORB (Sun and McDonough 1989). The trace elements are sorted by incompatibility in descending order. Zr contents have been determined by XRF, all others by ICP-MS. The range of magmas from Lesbos (Pe-Piper et al. 2014) and Samothraki (Vlahou et al. 2006) is shown in grey

Trace element composition

The analysed samples from Limnos are compared to shoshonitic rocks from Lesbos (Pe-Piper et al. 2014) and Samothraki (Vlahou et al. 2006) in a MORB-normalized incompatible element diagram (Sun and McDonough 1989; Fig. 4). The magmas from Limnos, Lesbos and Samothraki all show similar element patterns characterized by strong enrichments of Pb and the large ion lithophile elements (LILE) Cs, Rb and Ba compared to a depletion in the high field strength elements (HFSE) Nb, Ta, Zr and Ti. Yet, the shoshonitic samples are slightly more enriched in both element groups compared to high-K samples (Fig. 4). Uranium and Th are greatly enriched in all rocks, but the shoshonitic rocks show a slightly lower Th/U ratio than the high-K calc-alkaline samples, whereas the monzonites exhibit the highest Th/U ratios. All samples are enriched in the light rare earth elements (LREE) and gradually decrease in their contents towards the heavy rare earth elements (HREE), resulting in flat HREE patterns (Fig. 4). The samples further show a small negative Eu anomaly. One shoshonitic sample (LIM-45) has a stronger enrichment in middle and heavy REE. The Limnos magmas show the same correlation of increasing La/Sm and decreasing Ba/Th with SiO_2 as observed throughout the Aegean (Fig. 5a,b). However, the magmas of Limnos, Lesbos and Samothraki reach much higher La/Sm ratios compared to the SAVA. Within the samples of Limnos, the monzonites and many of the shoshonitic lavas have higher intermediate REE (Sm to Tb) contents, lower Ba/Th and higher Th/Nd than the high-K samples, whereas Nb/Zr shows no consistent variation among the magma series (Fig. 5b–d).

Radiogenic isotope composition

The age-corrected Sr, Nd and Pb isotope ratios of the Limnos magmas exhibit some of the highest $^{87}Sr/^{86}Sr$ and lowest $^{143}Nd/^{144}Nd$ and $^{206}Pb/^{204}Pb$ ratios (Fig. 6a,b) observed in Aegean magmatic rocks and resemble the magmas from Lesbos (Pe-Piper et al. 2014) and Samothraki (Vlahou et al. 2006). In contrast to the younger volcanic rocks of the SAVA (Bailey et al. 2009; Büttner et al. 2005; Elburg et al. 2018; Elburg and Smet 2020; Pe-Piper and Piper 1994), the Limnos magmas have higher $^{207}Pb/^{204}Pb$ and $^{208}Pb/^{204}Pb$ at lower $^{206}Pb/^{204}Pb$ (Fig. 6c,d). The majority of the Limnos magmas shows a relatively narrow range of Sr, Nd and Pb isotope ratios, that does not show any variation with increasing SiO_2 content (Fig. 5e,f). However, three samples show a distinctly different isotope composition. One high-K andesite from the Romanou unit has lower Pb isotope ratios, but higher $^{143}Nd/^{144}Nd$, while two dacites from the Myrina unit have lower $^{87}Sr/^{86}Sr$ and $^{207}Pb/^{204}Pb$, but higher $^{143}Nd/^{144}Nd$ and $^{206}Pb/^{204}Pb$ ratios (Fig. 6).

Discussion

Fractional crystallization processes affecting the Limnos magmas

The compositional trends of the magmatic rocks of Limnos resemble those of the SAVA lavas (Fig. 3) and probably reflect fractional crystallization, which has been suggested previously (Innocenti et al. 1994; Pe-Piper et al. 2009). The andesitic and dacitic rocks have similar radiogenic isotope and Nb/Zr ratios implying that they have closely

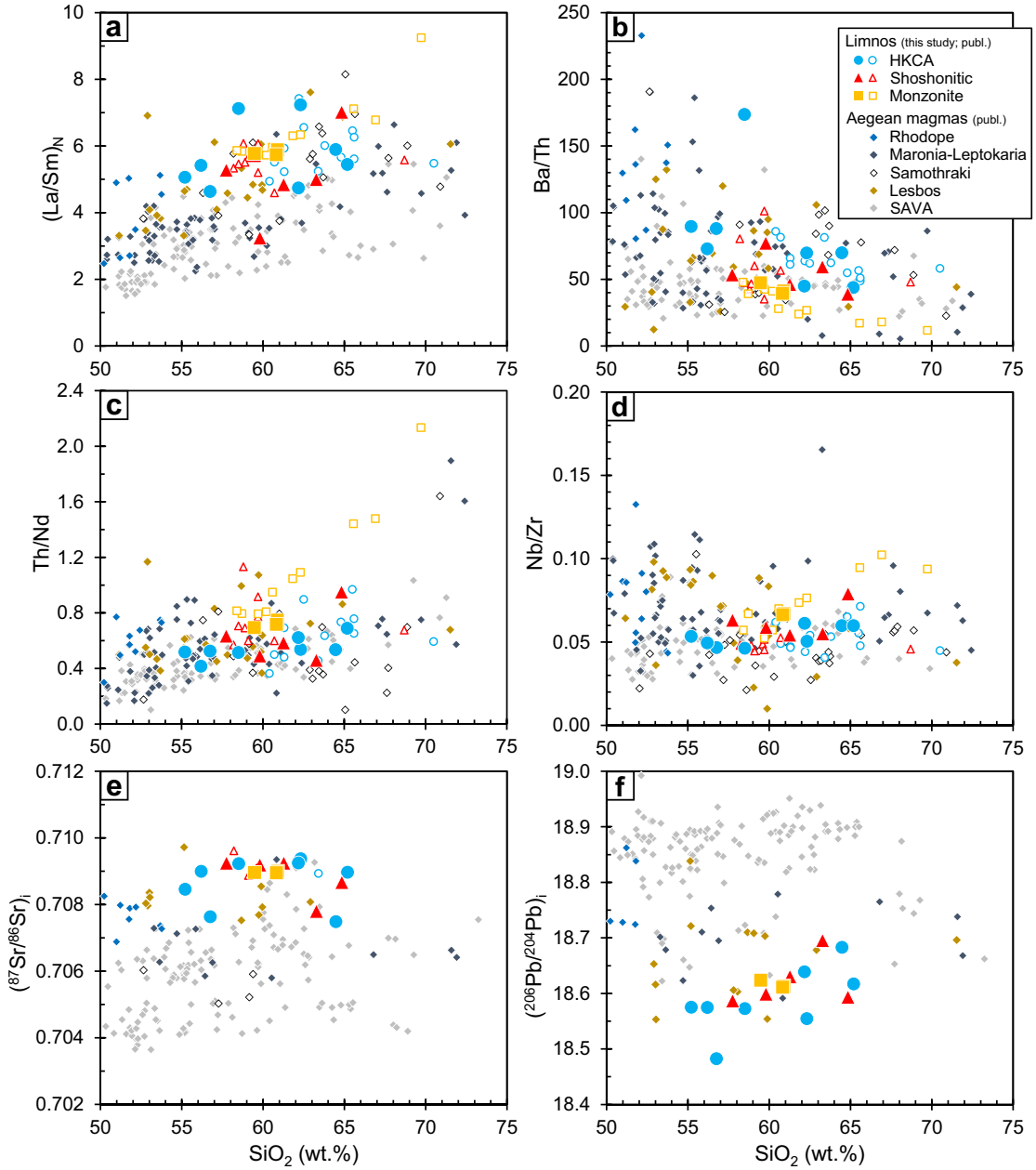

Fig. 5 (**a**–**d**) Incompatible element ratios vs. SiO_2. Nb/Zr ratios have been calculated using the Zr concentrations determined by XRF. (**e**,**f**) Initial $^{87}Sr/^{86}Sr$ and $^{206}Pb/^{204}Pb$ isotope ratios vs. SiO_2. Comparative data sets as in Fig. 3 with additional data sets from the Rhodope (Marchev et al. 2004) and Maronia-Leptokaria (Perkins et al. 2018; Schaarschmidt et al. 2021b)

related sources (Fig. 5d–f). Variable partial melting of crustal rocks and mixing with mantle-derived magmas would have caused significant changes in composition between andesites and dacites (e.g. Deschamps et al., 2017). The geothermometric calculations indicate that the samples record a large temperature range between 1130° and 700 °C (Fig. 2, Table 1) in agreement with conditions for extensive fractionation. The decrease in CaO and MgO with SiO_2 can be attributed to the fractionation of clinopyroxene, spinel and olivine at temperatures above 1000 °C and pressures of at least 0.5 GPa. Normal zoning patterns of plagioclase ranging from An54 to An20 in andesitic to dacitic lavas also reflect decreasing CaO contents during fractional crystallization. However, some of the variation of the bulk rock and mineral compositions may be due to magma mixing of closely related melts, which can also explain the abundance of subhedral plagioclase. The constant Al_2O_3, Sr and Eu contents with increasing SiO_2 indicate that plagioclase

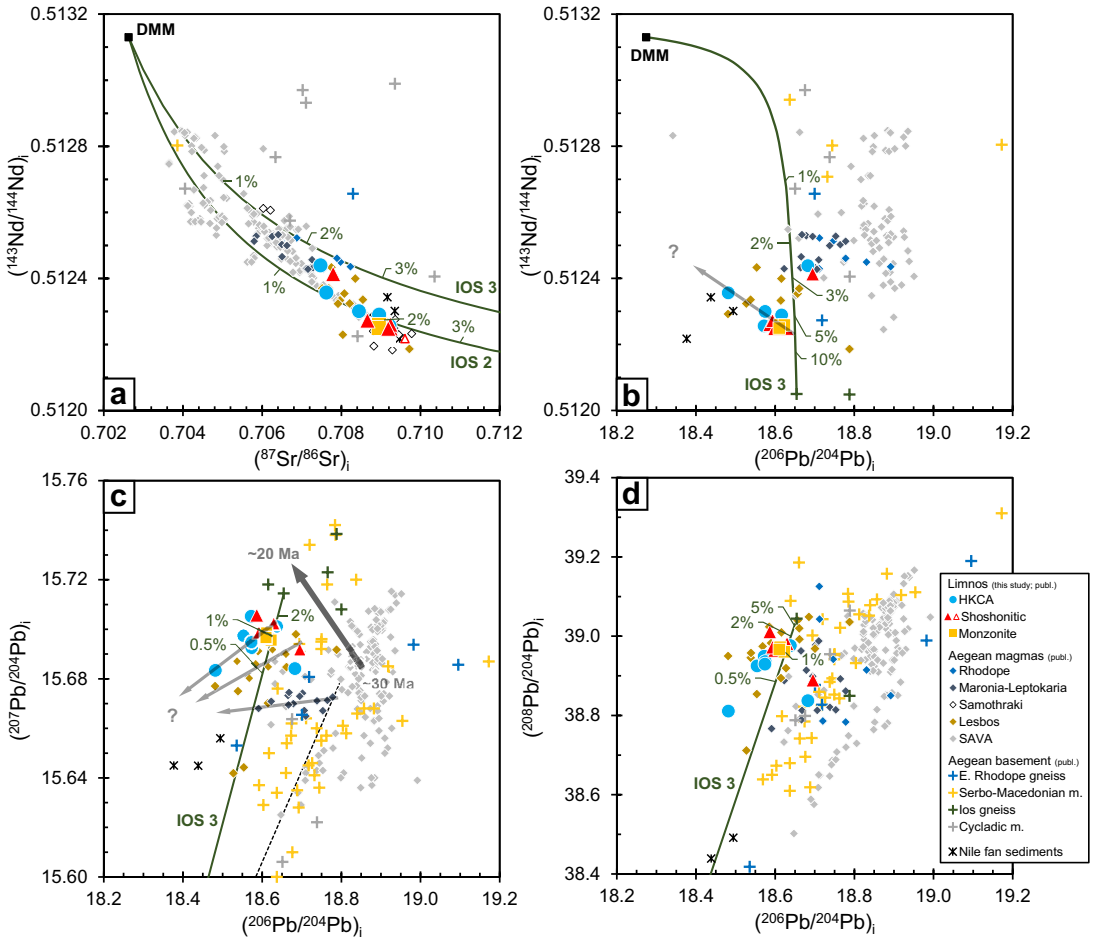

Fig. 6 (**a**–**d**) Initial radiogenic isotope ratios of Sr, Nd and Pb. For comparison, literature data of Limnos (Pe-Piper et al. 2009), Aegean basement rocks (Eastern Rhodope gneisses: Bonev et al. 2010; Serbo-Macedonian metamafics: Bonev et al. 2012 and Frei 1995; Cycladic metamafics: Stouraiti et al. 2017), Aegean magmas (Lesbos: Pe-Piper et al. 2014; Maronia: Schaarschmidt et al. 2021b; Rhodope: Marchev et al. 2004; Samothraki: Vlahou et al. 2006; SAVA: Bailey et al. 2009, Büttner et al. 2005, Elburg et al. 2018, Elburg and Smet 2020, Pe-Piper and Piper 1994) and Nile fan sediments (Klaver et al. 2015) are shown. Initial isotope ratios for basement samples were calculated for an age of 20 Ma. Mixing lines are shown between depleted MORB mantle (DMM: Workman and Hart 2005) and Ios gneiss (Büttner et al. 2005)

is not continuously fractionating from the melts probably due to high water contents which suppresses the crystallization of plagioclase during the early stage of fractionation (Almeev et al. 2012). Amphibole fractionation is indicated by decreasing FeO, MgO, Sc and Y concentrations. Ratios of light REE and middle/heavy REE also correlate positively with the SiO_2 content (Fig. 5a), which can be explained by fractional crystallization of amphibole and/or clinopyroxene. Fe-Ti oxide fractionation causes continuously decreasing FeO and TiO_2 contents which is in accordance with the relatively oxidizing conditions (FMQ + 2) calculated for magnetite-ilmenite pairs and amphiboles at ~ 900 to 730 °C. Apatite fractionation is reflected by decreasing P_2O_5 contents with increasing silica. Thus, the variation of major elements of the Limnos magmatic rocks is due to the crystallization and fractionation of olivine, clinopyroxene, amphibole, biotite, apatite and magnetite/ilmenite, whereas plagioclase fractionation is not observed during the early magma evolution. Mixing between related magmas within the two different magmatic series may have also contributed to the observed variation.

Innocenti et al. (1994) suggested that the variations in K_2O and other incompatible elements between high-K and shoshonitic lavas at Limnos reflect crystal fractionation processes at varying crustal depths from one parental magma. According to this model, fractionation of olivine, pyroxene, plagioclase, and magnetite at high pressures led to the formation of shoshonitic magmas, whereas fractionation of plagioclase, clinopyroxene, and magnetite at low pressures generated high-K melts. Geobarometric calculations

for clinopyroxene of the shoshonitic sample LIM-42 gave crystallization pressures of ~ 0.5 GPa which is similar to the pressures of the high-K samples (0.2 to 0.5 GPa for amphibole) and corresponds to a maximum crystallization depth of 18 km. The shoshonitic monzonite sample LIM-14 yields lower pressures of ~ 0.2 GPa for clinopyroxene and < 0.1 GPa for amphibole, which corresponds to a crystallization depth of ~ 5 km and an intrusion depth of ~ 2 km (Cas and Simmons 2018). Hence, these results do not support a model of systematically different pressures of crystallization for shoshonitic and high-K magmas. Rather, the lavas show variable pressures probably reflecting different magma stagnation levels and the monzonite represents a shoshonitic magma batch that crystallized in the upper crust. Additionally, the monzonites and many of the shoshonitic rocks have lower Ba/Th and higher Th/Nd and Nb/Yb compared to the high-K lavas (Fig. 5b,c) which implies different parental magmas for the magma series. High Th/Nd and Th/La ratios in magmatic rocks are often attributed to sediment subduction (Plank 1993, 2005), but the increasing Th/Nd and $(La/Sm)_N$ probably reflect the fractionation of amphibole which has very low Th/Nd < 0.1 and low $(La/Sm)_N < 1$ (Tiepolo et al. 2000; Schönhofen et al. 2020). An increasing Th/Nd by fractional crystallization is also in agreement with the constant $^{143}Nd/^{144}Nd$ (Fig. 5c), whereas assimilation would lead to changing Nd isotope ratios. We conclude that the shoshonitic and the high-K calc-alkaline rocks on Limnos have different parental magmas causing different crystal fractionation processes and liquid lines of descent.

Potential crustal assimilation in the Limnos magmas

The formation of shoshonitic magmas was suggested to be due to assimilation processes within the crust (e.g. Feeley and Cosca 2003), or to re-melting of lower crustal metabasalts by ascending basanitic magmas (Pe-Piper et al. 2009). We do not observe metamorphic xenoliths that would record assimilation of crustal rocks during the magma ascent. Metabasaltic rocks of the Cyclades, e.g. Samos, Paros and Naxos (Stouraiti et al. 2017), have too low Sr and Pb and too high Nd isotope ratios in order to be possible contaminants of the Limnos magmas. The metamorphic units of the Serbo-Macedonian massif have too high $^{143}Nd/^{144}Nd$ and $^{206}Pb/^{204}Pb$ (Bonev et al. 2012; Frei 1995) to represent a possible mixing end-member for the Limnos lavas (Fig. 6b). However, a sedimentary component is required to achieve the high incompatible element concentrations, the high Th/Nd and $(La/Sm)_N$, and high Pb-isotope ratios in the Limnos lavas (Spandler et al. 2007; Campbell et al. 2014). The constant Sr, Nd and Pb isotope ratios of the majority of Limnos rocks, including those with LOI > 5%, with increasing SiO_2 contents (Fig. 5e,f) do not indicate assimilation of continental crustal material which typically has $^{87}Sr/^{86}Sr > 0.710$ (e.g. Büttner et al. 2005; Stouraiti et al. 2010; Bonev et al. 2012). Additionally, the Th/Nd and $(La/Sm)_N$ of the Limnos samples are also constant with variable SiO_2 (Fig. 5c,d), but much higher than MORB (e.g. Th/Nd > 0.4 compared to 0.02 in N-MORB, Hofmann 1988), suggesting the contribution of partial melts from sediments to the primitive magmas. We conclude that the Limnos magmas are affected by a partial melt from a sedimentary end-member rather than by one from an amphibolitic source, but that this sediment component caused enrichment of the Limnos parental melts in the mantle rather than in the crust.

Origin of the Limnos parental melts

All magmatic rocks of Limnos are characterized by high Cs, Rb and Ba, while Nb and Ta show negative anomalies compared to N-MORB (Fig. 4), which is typical for a magma source that has been enriched by subduction components, for example, represented by lavas of the Aegean arc (Innocenti et al. (1994); Pe-Piper et al. (2009). The high Mg# (100*Mg/(Mg + Fe) > 60) in the basaltic andesites, the high Mg and Cr contents (Pe-Piper et al. 2009) and calculated eruption temperatures > 1100 °C, as well as the high water contents of ~ 5 wt.% in the lavas (Table 1) suggest a hydrous mantle origin of the parental melts (e.g. Arnaud et al. 1992). The enrichment of the mantle beneath Limnos causing high ratios of $(La/Sm)_N$ (> 4.5), Ba/Th (< 100), Th/Nb (~ 2.4), and $^{87}Sr/^{86}Sr$ require an influence of subducted sediments (Global Subducting Sediment: e.g. La/Sm ~ 5.0, Plank and Langmuir 1998) rather than fluids released from altered oceanic crust (Ba/Th ~ 600 to 2300 (< 1000 °C), Carter et al. 2015; Elliott 2003). Due to the complex history of the Aegean subduction system, it is challenging to identify the subducted units that affected the Limnos magmas at their time of formation. The magmatic activity on Limnos at 21 to 18 Ma (Pe-Piper et al. 2009) directly follows the partial accretion and subduction of the Apulian continental block after the closure of the Pindos ocean, as recorded by high-P metamorphic ages of 25 to 20 Ma for metamorphosed units of the Tripolitza and Ionian Blocks (Ring and Layer 2003; Ring et al. 2010). The isotope composition of northern Aegean magmatic rocks shows a shift from high $^{143}Nd/^{144}Nd$ and $^{206}Pb/^{204}Pb$ ratios (18.7 to 18.8) for ~ 30 Ma old magmas at Maronia-Leptokaria and in the Rhodope massif to lower $^{143}Nd/^{144}Nd$ and $^{206}Pb/^{204}Pb$ (18.5. to 18.6), but higher $^{207}Pb/^{204}Pb$ and $^{208}Pb/^{204}Pb$ ratios for the ~ 20 Ma old magmas at Limnos and Lesbos (Fig. 6c, dark arrow). We suggest that this variation of the Nd and Pb isotopes reflects the change from subduction of the Pindos oceanic crust overlain by pelagic or flysch sediments to subduction of the Apulian continental crust with Variscan basement overlain by Mesozoic–Cenozoic limestones, evaporites, pelagic sediments and flysch sediments (Sotiropoulos et al. 2003; Jolivet and

Brun 2010). Triassic to Oligocene limestones and evaporites have $^{87}Sr/^{86}Sr$ between 0.7068 and 0.7080 (e.g. Burke et al. 1982) and thus cannot cause the initial $^{87}Sr/^{86}Sr$ up to 0.7094 of the Limnos magmas. Therefore, we suggest that clastic sediments, such as arkosic sandstones and pelites derived from Variscan basement (Pe-Piper et al. 2021) are a more likely end-member in the source of the Limnos magmas. Due to the lack of trace element and Pb isotope data of sediments of the Apulian block, we cannot prove whether these sediments caused the shift towards low $^{143}Nd/^{144}Nd$ and $^{206}Pb/^{204}Pb$ but high $^{207}Pb/^{204}Pb$. However, published Pb isotope ratios of Cycladic basement units record low $^{143}Nd/^{144}Nd$ and $^{206}Pb/^{204}Pb$ with high $^{207}Pb/^{204}Pb$ ratios for metasedimentary gneisses from Ios (Büttner et al. 2005). Since the Ios gneiss underlies the Cycladic Blueschist Unit (Thomson et al. 2009) we speculate that it might resemble the subducted sediments of Apulia or the Variscan basement of which they were derived. Calculated mixing lines of average depleted mantle (i.e. DMM: depleted MORB mantle; Workman and Hart, 2005) with bulk Ios gneiss can roughly reproduce the Sr, Nd, and maximum Pb isotope ratios of the Limnos magmas (Fig. 6). The Pb isotopes require mixing of 1 to 2% Ios gneiss (IOS 3, Fig. 6c,d), whereas the Nd isotopes require mixing of 4 to 6% Ios gneiss (IOS 2, Büttner et al. 2005; Fig. 6b). However, the curvature of the mixing lines is also strongly affected by the Pb, Sr and Nd fractionation during the slab-to-mantle transfer, e.g. during sediment melting (e.g. Elliott 2003; Spandler et al. 2007). Thus, we suggest that the Ios gneiss represents a suitable end-member for the metasediments of the Apulian block that were subducted and caused the partial melting of the Limnos magmas in the mantle.

The Pb isotopes of Limnos rocks as well as those from Lesbos and Maronia-Leptokaria trend towards low $^{206}Pb/^{204}Pb$ ratios (Fig. 6c, small arrows). Decreasing $^{206}Pb/^{204}Pb$ ratios correlate with decreasing K/La, Rb/Ba, Nb/La (Fig. 7a–c) and P/Nd ratios within the Limnos samples. Especially the younger high-K lavas of the Myrina and northern Katalakon units show lower Rb and Nb concentrations and low $^{206}Pb/^{204}Pb$ ratios. The decreasing Nb/La ratios (Fig. 7c) and Nb concentrations at decreasing $^{206}Pb/^{204}Pb$ ratios exclude the influence of an enriched mantle component. It rather points towards a crustal component with low Rb, Th, K, Zr, and Nb concentrations (Fig. 7) that affected the source of the high-K Limnos magmas. Unradiogenic Pb and Hf isotopes have been observed for coarse-grained sediments at the African shelf (Klaver et al. 2015) or in the forearc of the Lesser Antilles (Carpentier et al. 2009) due to higher portions of detrital zircon. The Quaternary Nile fan sediments from the African shelf (Klaver et al. 2015) have lower K/La ratios (~ 130), LILE and LREE contents than the Limnos magmas (K/La ~ 500), which could explain some but not all of the decreasing element concentrations (Fig. 7).

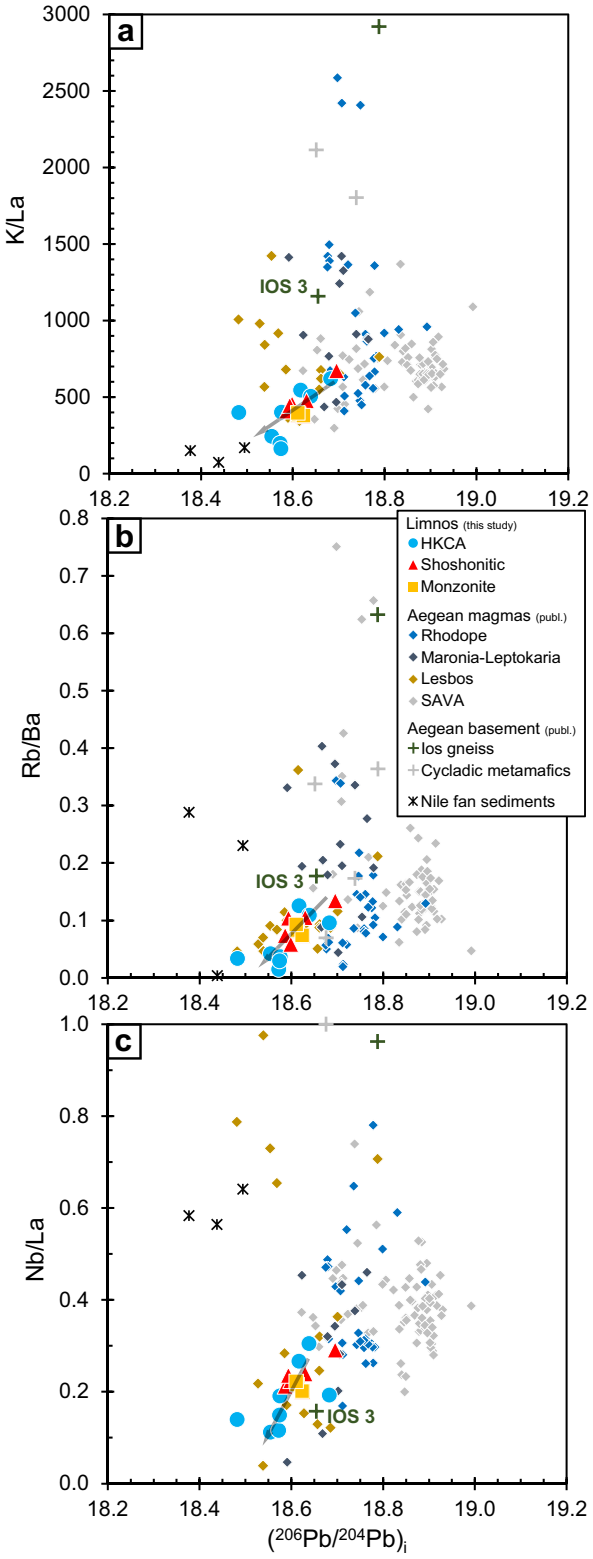

Fig. 7 (**a**–**c**) Initial $^{206}Pb/^{204}Pb$ isotope ratios vs. trace element ratios. Trends within the Limnos magmas show decreasing $^{206}Pb/^{204}Pb$ correlating with decreasing K/La, Rb/Ba and Nb/La ratios. Data sets of Aegean magmas (as in Fig. 5), Cycladic basement rocks (Büttner et al. 2005; Stouraiti et al. 2017) and Nile fan sediments (Klaver et al. 2015) are shown for comparison

Therefore the K/La variation in the Limnos magmas may be explained by a mixture of clastic sediments, such as arkoses and pelites (high K/La, low $^{143}Nd/^{144}Nd$), and more limestone-rich sediments (low K/La, higher $^{143}Nd/^{144}Nd$) derived from the subducted Apulian slab. We conclude that subduction of the Apulian sedimentary sequence and its interaction with the mantle wedge controlled the incompatible element composition and the Sr, Nd, and Pb isotope composition of the parental Limnos magmas. Interaction of mantle with slab-derived sediments or partial melts from the sediments generated a heterogenous source that gave rise to the high-K calc-alkaline and shoshonitic magmas.

Melting model for the Limnos parental melts

Experiments of Sekine and Wyllie (1983) simulated the reaction of granitic melt derived from sediments with mantle peridotite under P–T conditions reached in subduction zones. Their results suggest that hybrid reaction zones form in the mantle wedge that are characterized by orthopyroxene- and clinopyroxene-rich veins in the absence of olivine. Garnet, quartz and phlogopite might form as well, the latter being an important supplier of potassium to partial melts (Sekine and Wyllie 1983). More recent reaction experiments of sediment melt and dunite confirmed the formation of phlogopite-pyroxenites and K-rich magmas under P–T conditions of a subduction zone (1 GPa, < 1000 °C; Förster et al. 2019). Geochemical characteristics of western Anatolian volcanics resemble those of Limnos and were interpreted to be generated by melting of phlogopite-rich veins in subduction-metasomatized lithospheric mantle (Dilek and Altunkaynak 2010). Condamine and Médard (2014) also emphasized the importance of phlogopite for the generation of potassic magmas. The presence of residual phlogopite in the mantle is supported by low Ba/Rb, K/La, and high Rb/Sr ratios (Furman and Graham 1999) which we observe in the Limnos lavas (Fig. 7). Low CaO/Al_2O_3 (~0.29) and low contents of CaO (~4.5 wt.%) and Sc (~14 µg/g) in the Limnos samples can also be related to a phlogopite-bearing mantle source (Miller et al. 1999). Based on these findings we suggest that the source rock of the Limnos primary magmas was dominated by orthopyroxene, clinopyroxene and phlogopite. Melt contributions from surrounding peridotite can be considered relatively small, because of the much lower solidus temperature of pyroxenite at pressures < 1 GPa and with little involvement of released volatiles (Lambart et al. 2016).

We use REE modelling to test a potential melting regime of the Limnos magmas by comparing variable mixing endmembers and source mineralogies (Fig. 8). The composition of the hybridized mantle source for the melt modelling was determined by mixing DMM (Workman and Hart 2005) with up to 20% of sedimentary material (Fig. 8, solid lines). As sedimentary mixing endmember we use either bulk Ios gneiss (Büttner et al. 2005) or a sediment melt derived from melting experiments of a metapelitic starting material (Hermann and Rubatto 2009; run C-1578 at 900 °C, 3.5 GPa and 6% H_2O added). The resulting REE compositions were used for modelling non-modal batch melting at variable degrees of melting (Fig. 8, dashed lines). The partition coefficients used for the melting model are presented in Table 2. Comparing the REE ratios of the intermediate Limnos magmas (< 60 wt.% SiO_2) to the modelled compositions allows us to estimate the degree of partial melting and the influence of different source rock mineralogies (Fig. 8).

Condamine and Médard (2014) suggested the following melt reaction for a phlogopite-lherzolite above 1075 °C:

0.49phl + 0.56 opx + 0.47 cpx + 0.05 sp = 0.58 ol + 1.00 melt

(phl = phlogopite; opx = orthopyroxene; cpx = clinopyroxene; sp = spinel; ol = olivine).

Since olivine is consumed during the reaction between sediment melt and peridotite, the modified melt reaction for an olivine-free phlogopite-pyroxenite would be:

0.31phl + 0.36 opx + 0.30 cpx + 0.03 sp = 1.00 melt.

Small amounts of spinel (~ 1%) are negligible for the modelling due to their low distribution coefficients but have been included nevertheless as spinel is likely to occur as a minor or accessory mineral in mantle rocks at moderate pressures (~ 1 GPa). The REE concentrations of the Limnos magmas can be modelled by assuming the following composition for the hybridized mantle rock: 5% phl, 20% cpx, 74% opx, 1% sp (Fig. 8a). According to this model, the samples of Limnos require about 5 to 10% partial melting after mixing of DMM with either 10 to 20% of bulk Ios gneiss (Fig. 8a) or 2 to 5% of experimental sediment melt (Fig. 8b). The melting behaviour of this phlogopite-pyroxenite is compared to other typical mantle lithologies in Fig. 8b–d. Melting of spinel peridotite (Fig. 8c) shows similar melting curves to the phlogopite pyroxenite (Fig. 8a) but requires pretty low melting degrees < 4%. A garnet peridotite source may provide suitable Sm/Yb ratios even at low amounts of sedimentary material in the mixture (< 5%) but fails to reproduce the high La/Sm ratios of the Limnos magmas (Fig. 8d). We conclude that the REE contents of Limnos can be explained by 5 to 10% partial melting of a pyroxenite containing 5% phlogopite.

Most of the intermediate shoshonitic magmas of Limnos (< 60 wt.% SiO_2) differ from the high-K samples in having slightly higher middle REE concentrations and Sm/Yb ratios. A higher amount of sedimentary material could lead to a higher amount of phlogopite involved during partial melting, which at the same time increased the K content in the melt. Higher Nb/Yb, Th/Nd, Sm/Yb ratios and higher concentrations of Cs, Rb, Zr and U in most of the shoshonitic compared to the high-K magmas (Fig. 5) indicate that both, a variable input of sedimentary material and variable

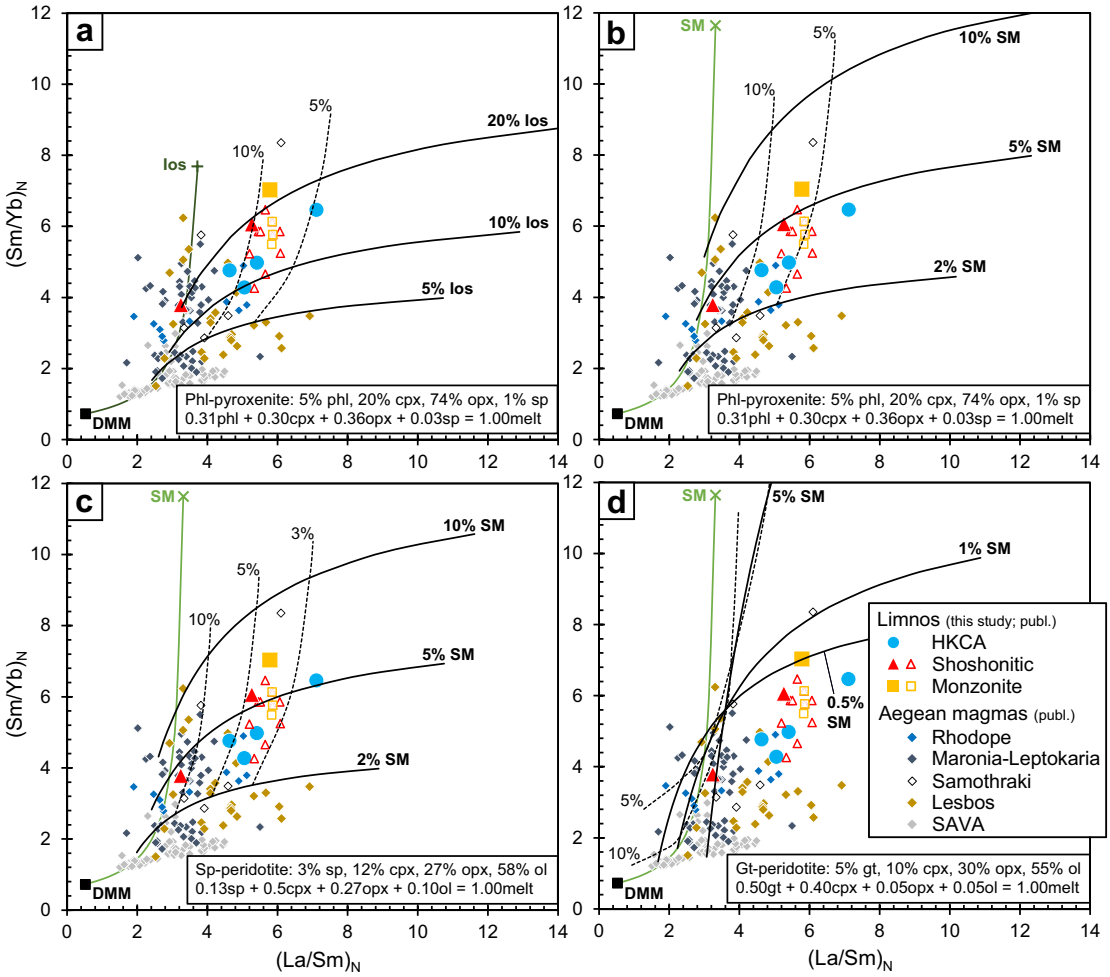

Fig. 8 Chondrite normalized La/Sm vs. Sm/Yb ratios for Limnos and Aegean magmas with $SiO_2 < 60$ wt.%. For references see Fig. 5. Melting curves are shown for different potential source rock mixtures of depleted MORB mantle (DMM, Workman and Hart 2005) and a crustal slab component (Ios gneiss or sediment melt (SM), bold lines) at variable partial melting degrees (dashed lines). The modal amounts of the minerals in the source and involved in the melting is given in the box. Abbr.: phl = phlogopite, cpx = clinopyroxene, opx = orthopyroxene, sp = spinel, gt = garnet, ol = olivine (**a**) Phlogopite pyroxenite: DMM-Ios gneiss mixture; melt reaction modified after Condamine and Médard (2014). (**b**) Phlogopite pyroxenite: DMM-sediment melt mixture. (**c**) Spinel peridotite: DMM-sediment melt mixture; melt reaction after Thirlwall et al. (1994). (**d**) Garnet peridotite: DMM-sediment melt mixture

melting degrees controlled the formation of shoshonitic vs. high-K magmas. This is in accordance with models from the Maronia-Leptokaria high-K calc-alkaline to shoshonitic rocks where it is believed that variable source enrichment by subducted sediments caused lower water contents and lower degrees of melting at higher temperatures for shoshonitic relative to high-K calc-alkaline magmas (Perkins et al. 2018; Schaarschmidt et al. 2021b). This agrees with lower water contents estimated in the Limnos shoshonitic compared to the high-K lavas (Table 1). Yet, in contrast to the Maronia–Leptokaria magmas, magmatism at Limnos evolves with time from dominantly shoshonitic magmatism at southern Katalakon and Romanou (22.3 ± 0.7 Ma) to younger (21–18 Ma) high-K magmatism at northern Katalakon and Myrina (Pe-Piper et al. 2009). Whereas the previous melting model of the Limnos magmas assumed a source of metabasaltic amphibolite (Pe-Piper et al. (2009), our new model suggests a pyroxenitic source that can explain the high Sr/Y and Sr concentrations in Limnos samples (~ 1000 µg/g), i.e. partial melting of a plagioclase-free source (Castillo 2012). This new model is in agreement with the massive subduction of sedimentary material at the time of magmatic activity on Limnos.

Tectonic framework of the Limnos magmatic system

The formation of the Miocene Limnos magmas has been related on one hand to the subduction at the southwards

Table 2 Selected partition coefficients for clinopyroxene (cpx), orthopyroxene (opx), olivine (ol), garnet (gt) and spinel (sp) used for the modelling of equilibrium melting

		D_{cpx}	D_{opx}	D_{ol}	D_{phl}	D_{gt}	D_{sp}
Phl-pyroxenite	La	0.043[a]	0.003[a]	–	0.0413[b]	–	0.0006[c]
	Sm	0.363[a]	0.021[a]	–	0.0255[b]	–	0.001[c]
	Yb	0.543[a]	0.164[a]	–	0.0484[b]	–	0.0045[c]
Gt-peridotite	La	0.043[a]	0.003[a]	0.0000082[d]	–	0.001[e]	–
	Sm	0.363[a]	0.021[a]	0.00086[d]	–	0.25[e]	–
	Yb	0.543[a]	0.164[a]	0.036[d]	–	6.6[e]	–
Sp-peridotite	La	0.071[d]	0.0008[d]	0.0000082[d]	–	–	0.0006[c]
	Sm	0.459[d]	0.0251[d]	0.00032[d]	–	–	0.001[c]
	Yb	0.76[d]	0.168[d]	0.0096[d]	–	–	0.0045[c]

[a]McDade et al. (2003a)
[b]Fujimaki et al. (1984)
[c]Stracke et al. (2003)
[d]McDade et al. (2003b)
[e]Johnson (1998)

migrating Aegean volcanic arc (Innocenti et al. 1994), and on the other hand to post-orogenic slab detachment and asthenospheric upwelling (Pe-Piper et al. 2009). Thus, the tectonic situation of the Limnos region at the time of magmatic activity needs to be considered to understand the cause of partial melting. Limnos largely consists of Eocene to Oligocene clastic flysch sediments representing deposits of an accretionary wedge in the fore-arc region of the Oligocene magmatic arc situated in the Rhodopes (Görür and Okay 1996; Maravelis et al. 2016). The Limnos volcanic rocks largely rest on marine clastic sediments of the Late Oligocene to Early Miocene Ifestia Unit that show an erosional top and are overlain by the continental Therma Unit implying rapid uplift (Innocenti et al. 2009). An interpretation of the fault systems on Limnos indicates that this uplift is probably due to Middle Oligocene to Early Miocene collision between Apulia and Eurasia (Innocenti et al. 1994; Tranos 2009). Thus, the setting of the Limnos magmatic activity in the Oligocene closely resembled that of the presently active SAVA with rapid vertical movements due to changes in the dynamics of the fore-arc and arc region of the migrating subduction zone. Tectonic reconstructions also suggest that the active volcanic arc was close to the Limnos region 23 million years ago (Faccenna et al. 2014). Seismic data show an unusually thick lithosphere of possibly 150 km beneath the northern Aegean (Sodoudi et al. 2006), i.e. there is no indication of asthenospheric upwelling and lithospheric thinning beneath Limnos. Furthermore, the isotopic and trace element composition of the Limnos magmas reveals melting of a heterogeneous, hydrous mantle source that was affected by slab-derived crustal components. We conclude that the magmatism of Limnos reflects partial melting above the subducting slab and its southward-directed rollback that caused migration of the magmatic activity (Innocenti et al. 1994; Schaarschmidt et al. 2021a).

The tectonic models of the Aegean subduction zone suggest accretion and partial subduction of continental blocks belonging to the Apulian block during Oligocene and a change to subduction of the oceanic lithosphere of the eastern Mediterranean ~ 23 Ma ago (Ring et al. 2010; Jolivet et al. 2013). Thus, at the time of magma formation beneath Limnos between 22 and 18 Ma, significant volumes of continental crustal material of the Apulia block were already subducted and have likely affected the mantle wedge causing the extreme isotopic compositions of Upper Miocene Aegean magmas. The processes at the Oligocene–Miocene North Aegean arc may have resembled those occurring at the Banda Arc where parts of the Australian continental lithosphere are subducted causing extreme element enrichments in arc magmas (e.g. Elburg et al. 2005), whereas other lithospheric parts are accreted (Harris 2011). Additionally, the subduction of the continental lithospheric blocks causes uplift in the Banda Arc (Harris 2011) which is consistent with the uplift observed in the sediment succession of Limnos prior to and during the magmatic activity (Innocenti et al. 1994). We conclude that the magmatic and tectonic evolution of Limnos can be explained by the subduction of continental material of the Apulian block and we present the first comprehensive model for the geologic processes in this part of the northern Aegean.

Conclusions

The high-K calc-alkaline to shoshonitic trachyandesites and the Fakos monzonite are genetically related and underwent fractional crystallization at temperatures of 1100 to 700 °C and pressures around 0.5 to 0.1 GPa with no detectable crustal contamination. Mixing of different related magma batches can have also affected the composition of the lavas.

The radiogenic isotope and incompatible element compositions of the Limnos magmatic rocks indicate the input of a continental sediment component to the depleted mantle wedge, and this component changed from that previously observed in older rocks from the northern Aegean. We suggest that Mesozoic–Cenozoic sediments of the Apulian block contributed to the source and controlled the trace element and isotope signature of the parental magmas, in accordance with upper Miocene ages of the high-pressure metamorphism of the respective units. This highlights the change of sedimentary input into the Aegean subduction zone between 30 and 20 million years ago. The subducted sedimentary component interacted with the mantle rock to form enriched phlogopite-pyroxenite veins at the expense of olivine. Partial melting of this phlogopite-pyroxenite source at degrees of 5 to 10% and varying sediment input into the mantle cause variations between high-K and shoshonitic rocks on Limnos. The magmatic rocks of Limnos indicate that both the melting processes in the mantle wedge and the complex variation of subducted oceanic and continental units in the migrating Aegean arc caused considerable changes in magma composition.

Supplementary Information The online version contains supplementary material available at https://doi.org/10.1007/s00410-022-01940-7.

Acknowledgements We thank M. Hertel for her help with the sample preparation process and the XRF analysis and M. Regelous for the measurements of trace elements and isotope ratios by ICPMS and TIMS. We gratefully acknowledge the constructive reviews by G. Pe-Piper and an anonymous reviewer that considerably improved the quality of this work.

Funding Open Access funding enabled and organized by Projekt DEAL.

Declarations

Conflict of interests Funding of the project was provided by the GeoZentrum Nordbayern which is gratefully acknowledged. The authors have no relevant financial or non-financial interests to disclose.

References

Aldanmaz E, Pearce JA, Thirlwall MF, Mitchell JG (2000) Petrogenetic evolution of late Cenozoic post-collision volcanism in western anatolia, Turkey. J Volcanol Geoth Res 102:67–95

Almeev R, Holtz F, Koepke J, Parat F (2012) Experimental calibration of the effect of H2O on plagioclase crystallization in basaltic melt at 200 MPa. Am Miner 97:1234–1240

Andersen DJ, Lindsley DH (1985) New (and final) models for the Ti-magnetite/ilmenite geothermometer and oxygen barometer. Am Geophys Union 66(18):416

Armijo R, Meyer B, Hubert A, Barka A (1999) Westward propagation of the north Anatolian fault into the northern Aegean: timing and kinematics. Geology 27:267–270

Arnaud NO, Vidal P, Tapponier P, Matte P, Deng WM (1992) The high K20 volcanism of northwestern Tibet: geochemistry and tectonic implications. Earth Planet Sci Lett 111:351–367

Bailey JC, Jensen ES, Hansen A, Kann AD, Kann K (2009) Formation of heterogeneous magmatic series beneath North Santorini, South Aegean island arc. Lithos 110:20–36

Behn MD, Kelemen PB, Hirth G, Hacker BR, Massonne HJ (2011) Diapirs as the source of the sediment signature in arc lavas. Nat Geosci 4:641–646

Bonev N, Moritz R, Márton I, Chiaradia M, Marchev P (2010) Geochemistry, tectonics and crustal evolution of basement rocks in the Eastern Rhodope Massif, Bulgaria. Int Geol Rev 52:269–297

Bonev N, Dilek Y, Hanchar JM, Bogdanov K, Klain L (2012) Nd–Sr–Pb isotopic composition and mantle sources of Triassic rift units in the Serbo-Macedonian and the western Rhodope massifs (Bulgaria–Greece). Geol Mag 149(1):146–152

Brun JP, Sokoutis D (2010) 45 my of Aegean crust and mantle flow driven by trench retreat. Geology 38(9):815–818

Brun JP, Faccenna C, Gueydan F, Sokoutis D, Philippon M, Kydonakis K, Gorini C (2016) The two-stage Aegean extension, from localized to distributed, a result of slab rollback acceleration. Can J Earth Sci 53(11):1142–1157

Burke WH, Denison RE, Hetherington EA, Koepnick RB, Nelson HF, Otto JB (1982) Variation of seawater 87Sr/86Sr throughout Phanerozoic time. Geology 10:516–519

Büttner A, Kleinhanns IC, Rufer D, Hunziker JC, Villa IM (2005) Magma generation at the easternmost section of the Hellenic arc: Hf, Nd, Pb and Sr isotope geochemistry of Nisyros and Yali volcanoes. Lithos 83:29–46

Campbell IH, Stepanov AS, Liang HY, Allen CM, Norman MD, Zhang YQ, Xie YW (2014) The origin of shoshonites: new insights from the Tertiary high-potassium intrusions of eastern Tibet. Contrib Miner Petrol 167:983

Caracciolo L, Critelli S, Innocenti F, Kolios N, Manetti P (2011) Unravelling provenance from Eocene-Oligocene sandstones of the Thrace Basin, North-east Greece. Sedimentology 58:1988–2011

Carpentier M, Chauvel C, Maury RC, Mattielli N (2009) The "zircon effect" as recorded by the chemical and Hf isotopic compositions of lesser antilles forearc sediments. Earth Planet Sci Lett 287(1–2):86–99

Carter LB, Skora S, Blundy JD, De Hoog JCM, Elliott T (2015) An experimental study of trace element fluxes from subducted oceanic crust. J Petrol 56(8):1585–1606

Cas RA, Simmons J (2018) Why deep-water eruptions are so different from subaerial eruptions. Front Earth Sci 6:198

Castillo PR (2012) Adakite petrogenesis. Lithos 134–135:304–316

Çelik ÖF, Marzoli A, Marschik R, Chiaradia M, Neubauer F, Öz İ (2011) Early–middle Jurassic intra-oceanic subduction in the İzmir-Ankara-Erzincan Ocean, northern Turkey. Tectonophysics 509(1–2):120–134

Compston W, Oversby VM (1969) Lead isotopic analysis using a double spike. J Geophys Res 74(17):4338–4348
Condamine P, Médard E (2014) Experimental melting of phlogopite-bearing mantle at 1 GPa: implications for potassic magmatism. Earth Planet Sci Lett 397:80–92
Davidson JP, Hora JM, Garrson J, Dungan MA (2005) Crustal forensics in arc magmas. J Volcanol Geoth Res 140:157–170
Deschamps F, Duchene S, de Sigoyer J, Bosse V, Benoit M, Vanderhaege O (2017) Coeval mantle-derived and crust-derived magmas forming two neighbouring plutons in the Songpan Ganze accretionary orogenic wedge (SW China). J Petrol 58(11):2221–2256
Dilek Y, Altunkynak S (2010) Geochemistry of Neogene-Quaternary alkaline volcanism in western Anatolia, Turkey, and implications for the Aegean mantle. Int Geol Rev 52:631–655
Elburg MA, Smet I (2020) Geochemistry of lavas from aegina and poros (Aegean Arc, Greece): distinguishing upper crustal contamination and source contamination in the Saronic Gulf area. Lithos 358–359:105416
Elburg MA, van Bergen MJ, Foden JD (2004) Subducted upper and lower continental crust contributes to magmatism in the collision sector of the Sunda-Banda arc, Indonesia. Geology 32:41–44
Elburg MA, Foden JD, van Bergen MJ, Zulkarnain I (2005) Australia and Indonesia in collision: geochemical sources of magmatism. J Volcanol Geoth Res 140(1–3):25–47
Elburg MA, Smet I, De Pelsmaeker E (2014) Influence of source materials and fractionating assemblage on magmatism along the Aegean Arc, and implications for crustal growth. Geol Soc Lond Spec Publ 385(1):137
Elburg MA, Smet I, Van den Haute P, Vanhaecke F, Klaver M, Andersen T (2018) Extreme isotopic variation documents extensional tectonics in arc magmas from Methana, Greece. Lithos 318–319:386–398
Elliott T (2003) Tracers of the slab. Geophys Monogr Ser 238:23–45
Erbil Ü, Okay AI, Hakyemez A (2021) Late oligocene-early miocene shortening in the Thrace Basin, northern Aegean. Int J Earth Sci 110(6):1921–1936
Fabbro G, Druitt TH, Scaillet S (2013) Evolution of the crustal magma plumbing system during the build-up to the 22-ka caldera-forming eruption of Santorini (Greece). Bull Volcanol 75(12):1–22
Faccenna C, Brun JP (2008) Exhumation of high-pressure rocks driven by slab-rollback. Earth Planet Sci Lett 272:1–7
Faccenna C, Becker TW, Auer L, Billi A, Boschi L, Brun JP et al (2014) Mantle dynamics in the Mediterranean. Rev Geophys 52(3):283–332
Feeley TC, Cosca MA (2003) Time vs. composition trends of magmatism at sunlight volcano, Absaroka volcanic province. Wyoming Geol Soc Am Bull 115:714–728
Foley SF (1992) Vein-plus-wall-rock melting mechanisms in the lithosphere and the origin of potassic alkaline magmas. Lithos 28(3–6):435–453
Fornadel AP, Voudouris PC, Spry PG, Melfos V (2012) Mineralogical, stable isotope, and fluid inclusion studies of spatially related porphyry Cu and epithermal Au-Te mineralization, Fakos Peninsula, Limnos Island, Greece. Miner Petrol 105:85–111
Förster MW, Prelevic D, Buhre S, Mertz-Kraus R, Foley SF (2019) An experimental study of the role of partial melts of sediments versus mantle melts in the sources of potassic magmatism. J Asian Earth Sci 177:76–88
Frei R (1995) Evolution of mineralizing fluid in the porphyry copper system of the Skouries deposit, Northeast Chalkidiki (Greece); evidence from combined Pb-Sr and stable isotope data. Econ Geol 90(4):746–762
Fujimaki H, Tatsumoto M, Aoki KI (1984) Partition coefficients of Hf, Zr, and REE between phenocrysts and groundmasses. J Geophys Res 89:662–672
Furman T, Graham D (1999) Erosion of lithospheric mantle beneath the East African Rift system: geochemical evidence from the Kivu volcanic province. Lithos 48:237–262
Görür N, Okay AI (1996) A fore-arc origin for the Thrace Basin, NW Turkey. Geol Rundsch 85:662–668
Govindaraju K (1994) Compilation of working values and sample description for 383 geostandards. Geostandard Newslett 18:1–158
Harris M (2011) The accretion of lower oceanic crust. Dissertation, University of Southampton
Hawkesworth CJ, Gallagher K, Hergt JM, McDermott F (1993) Mantle and slab contributions in arc magmas. Ann Rev Earth Planet Sci 21:175–204
Hermann J, Rubatto D (2009) Accessory phase control on the trace element signature of sediment melts in subduction zones. Chem Geol 265:512–526
Hofmann AW (1988) Chemical differentiation of the earth: the relationship between mantle continental crust, and oceanic crust. Earth Planet Sci Lett 90:297–314
Innocenti F, Manetti P, Peccerillo A, Poli G (1981) South Aegean volcanic arc: geochemical variations and geotectonic implications. Bull Volcanologique 44(3):377–391
Innocenti F, Manetti P, Mazzuoli R, Pertusati P, Fytikas M, Kolios N (1994) The geology and geodynamic significance of the Island of Limnos, North Aegean Sea, Greece. Neues Jb Geol 11:661–691
Innocenti F, Manetti P, Mazzuoli R, Pertusati P, Fytikas M, Kolios N et al (2009) Geological map (scale 1:50,000) of limnos island (Greece): explanatory notes. Acta Vulcanol 21(1–2):123–134
Jochum KP, Weis U, Schwager B, Stoll B, Wilson SA, Haug GH et al (2016) Reference values following ISO guidelines for frequently requested rock reference materials. Geostand Geoanal Res 40(3):333–350
Johnson KT (1998) Experimental determination of partition coefficients for rare earth and high-field-strength elements between clinopyroxene, garnet, and basaltic melt at high pressures. Contrib Miner Petrol 133:60–68
Jolivet L, Brun JP (2010) Cenozoic geodynamic evolution of the Aegean. Int J Earth Sci 99:109–138
Jolivet L, Faccenna C, Huet B, Labrousse L, Le Pourhiet L (2013) Aegean tectonics: strain localisation, slab tearing and trench retreat. Tectonophys Elsevier 597–598:1–33
Jolivet L, Menant A, Sternai P, Rabillard A, Arbaret L, Augier R (2015) The geological signature of a slab tear below the Aegean. Tectonophysics 659:166–182
Karabulut H, Paul A, Özbakir AD, Ergün T, Sentürk S (2019) A new crustal model of the Anatolia-Aegean domain: evidence for the dominant role of isostasy in the support of the Anatolian plateau. Geophys J Int 218:57–73
Kelemen PB (1995) Genesis of high Mg# andesites and the continental crust. Contrib Miner Petrol 120(1):1–19
Kirchenbaur M, Münker C, Schuth S, Garbe-Schönberg D (2012) Tectonomagmatic constraints on the sources of Eastern Mediterranean K-rich lavas. J Petrol 53(1):27–65
Klaver M, Djuly T, de Graaf S (2015) Temporal and spatial variations in provenance of Eastern Mediterranean Sea sediments: implications for Aegean and Aeolian arc volcanism. Geochim Cosmochim Acta 153:149–168
Koukouvelas IK, Aydin A (2002) Fault structure and related basins of the North Aegean Sea and its surroundings. Tectonics 21:5
Kushiro I (2007) Origin of magmas in subduction zones: a review of experimental studies. Proc Jpn Acad Ser B 83:1–15
Kydonakis K, Brun JP, Sokoutis D (2015) North Aegean core complexes, the gravity spreading of a thrust wedge. J Geophys Res: Solid Earth 120:595–616
Lambart S, Baker MB, Stolper EM (2016) The role of pyroxenite in basalt genesis: Melt-PX, a melting parameterization for

mantle pyroxenites between 0.9 and 5 GPa. J Geophys Res 121(8):5708–5735
Leake BE, Woolley AR, Arps CE, Birch WD, Gilbert MC, Grice J et al (1997) Nomenclature of amphiboles: report of the subcommitte on amphiboles of the International Mineralogical Association, Commission on New Minerals and Mineral Names. Am Min 82:1019–1037
Lepage LD (2003) ILMAT: an excel worksheet for ilmenite–magnetite geothermometry and geobarometry. Comp Geosci 29(5):673–678
Maravelis AG, Boutelier D, Catuneanu O, Seymour KS, Zelilidis A (2016) A review of tectonics and sedimentation in a forearc setting: hellenic Thrace Basin, North Aegean Sea and Northern Greece. Tectonophysics 674:1–19
Marchev P, Raicheva R, Downes H, Vaselli O, Chiaradia M, Moritz R (2004) Compositional diversity of Eocene-Oligocene basaltic magmatism in the Eastern Rhodopes, SE Bulgaria: implications for genesis and tectonic setting. Tectonophysics 393:301–328
Marroni M, Frassi C, Göncüoglu MC, Di Vincenzo G, Pandolfi L, Rebay G et al (2014) Late Jurassic amphibolite-facies metamorphism in the Intra-Pontide Suture Zone (Turkey): an eastward extension of the Vardar Ocean from the Balkans into Anatolia? J Geol Soc 171:605–608
Marschall HR, Schumacher JC (2012) Arc magmas sourced from mélange diapirs in subduction zones. Nat Geosci 5:862–867
McCulloch MT, Gamble JA (1991) Geochemical and geodynamical constraints on subduction zone magmatism. Earth Planet Sci Lett 102(3–4):358–374
McDade P, Blundy JD, Wood BJ (2003a) Trace element partitioning between mantle wedge peridotite and hydrous MgO-rich melt. Am Miner 88:1825–1831
McDade P, Blundy JD, Wood BJ (2003b) Trace element partitioning on the Tinaquillo Lherzolite solidus at 1.5 GPa. Phys Earth Planet in 139:129–147
Menant A, Jolivet L, Vrielynck B (2016) Kinematic reconstructions and magmatic evolution illuminating crustal and mantle dynamics of the eastern Mediterranean region since the late Cretaceous. Tectonophysics 675:103–140
Miller C, Schuster R, Klötzli U, Frank W, Purtscheller F (1999) Post-collisional potassic and ultrapotassic magmatism in SW Tibet: Geochemical and Sr–Nd–Pb–O isotopic constraints for mantle source characteristics and petrogenesis. J Petrol 40(9):1399–1424
Miyashiro A (1974) Volcanic rock series in island arcs and active continental margins. Am J Sci 274:321–355
Mutch EJ, Blundy JD, Tattitch BC, Cooper FJ, Brooker RA (2016) An experimental study of amphibole stability in low-pressure granitic magmas and a revised Al-in-hornblende geobarometer. Contrib Miner Petrol 171:85
Nicholls IA (1971) Petrology of santorini volcano, Cyclades. Greece J Petrol 12(1):67–119
Pavlides S, Tsapanos T, Zouros N, Sboras S, Koravos G, Chatzipetros A (2009) Using active fault data for assessing seismic hazard: A case study from NE Aegean Sea, Greece. In: Earthq Geotech Eng Satell Conf, 17th Int Conf Soil Mech Geotech Eng, Alexandria, Egypt 1–14
Peccerillo A, Taylor SR (1976) Geochemistry of the Eocene calc-alkaline volcanic rocks in the Kastamonu area, northern Turkey. Contrib Miner Petrol 58:63–81
Pe-Piper G, Piper DJ (1992) Geochemical variation with time in the Cenozoic high-K volcanic rocks of the island of Lesbos, Greece: significance for shoshonite petrogenesis. J Volcanol Geoth Res 53:371–387
Pe-Piper G, Piper DJ (1994) Miocene magnesian andesites and dacites, Evia, Greece: adakites associated with subducting slab detachment and extension. Lithos 31:125–140
Pe-Piper G, Piper D, Kokouvelas I, Dolansky L, Kokkalas S (2009) Postorogenic shoshonitic rocks and their origin by melting underplated basalts: The Miocene of Limnos, Greece. Geol Soc Am Bull 121:39–54
Pe-Piper G, Zhang Y, Piper DJ, Prelevic D (2014) Relationship of Mediterranean type lamproites to large shoshonite volcanoes, Miocene of Lesbos, NE Aegean Sea. Lithos 184–187:281–299
Pe-Piper G, Piper DJ, Bourli N, Zelilidis A (2021) Evolution of sedimentary basins as recorded in silica concretions: an example from the Ionian Zone. Western Greece Miner 11:763
Perkins R, Cooper F, Condon D, Tattitch B, Naden J (2018) Post-collisional cenozoic extension in the northern Aegean: the high-K to shoshonitic intrusive rocks of the Maronia Magmatic Corridor, northeastern Greece. Lithosphere 10:582–601
Perrin A, Goes S, Prytulak J, Rondenay S, Davies DR (2018) Mantle wedge temperatures and their potential relation to volcanic arc location. Earth Planet Sci Lett 501:67–77
Plank T (2005) Constraints from Thorium/Lanthanum on sediment recycling at subduction zones and the evolution of the continents. J Petrol 46(5):921–944
Plank T, Langmuir CH (1998) The chemical composition of subducting sediment and its consequences for the crust and mantle. Chem Geol 145:325–394
Plank T (1993) Mantle melting and crustal recycling in subduction zones. Dissertation, Columbia University, New York
Powell R, Powell M (1977) Geothermometry and oxygen barometry using coexisting iron-titanium oxides: a reappraisal. Mineral Mag 41(318):257–263
Putirka KD, Mikaelian H, Ryerson F, Shaw H (2003) New clinopyroxene-liquid thermobarometers for mafic, evolved, and volatile-bearing lava compositions, with applications to lavas from Tibet and the Snake River Plain. Idaho Am Miner 88(10):1542–1554
Ridolfi F, Renzulli A, Puerini M (2010) Stability and chemical equilibrium of amphibole in calc-alkaline magmas: an overview, new thermobarometric formulations and application to subduction-related volcanoes. Contrib Miner Petrol 160:45–66
Ring U, Layer PW (2003) High-pressure metamorphism in the Aegean, eastern Mediterranean: underplating and exhumation from the Late Cretaceous until the Miocene to Recent above the retreating Hellenic subduction zone. Tectonics 22(3):1022
Ring U, Layer PW, Reischmann T (2001) Miocene high-pressure metamorphism in the Cyclades and Crete, Aegean Sea, Greece: evidence for large-magnitude displacement on the Cretan detachment. Geology 29(5):395–398
Ring U, Glodny J, Will TM, Thomson SN (2010) The Hellenic subduction system: High-pressure metamorphism, exhumation, normal faulting, and large-scale extension. Ann Rev Earth Planet Sci 38:45–76
Robert U, Foden J, Varne R (1992) The Dodecanese Province, SE Aegean: a model for tectonic control on potassic magmatism. Lithos 28:241–260
Schaarschmidt A, Haase KM, Voudouris PC, Melfos V, Klemd R (2021a) Migration of arc magmatism above mantle wedge diapirs with variable sediment contribution in the Aegean. Geochem Geophys Geosyst 22(6):1–21
Schaarschmidt A, Klemd R, Regelous M, Voudouris P, Melfos V, Haase KM (2021b) The formation of shoshonitic magma and its relationship to porphyry-type mineralisation: the Maronia pluton in NE Greece. Lithos 380–381:105911
Schmidt MW, Jagoutz O (2017) The global systematics of primitive arc melts. Geochem Geophys Geosyst 18(8):2817–2854
Schönhofen MV, Haase KM, Beier C, Woelki D, Regelous M (2020) Chemical evolution of calc-alkaline magmas during the ascent through continental crust: constraints from Methana. Aegean Arc J Petrol 61(3):1–30

Sekine T, Wyllie PJ (1983) Experimental simulation of mantle hybridization in subduction zones. J Geol 91:511–528
Seymour KS, Lalonde A (1991) Monitoring oxygen fugacity conditions in pre-, syn- and postcaldera magma chamber of Nisyros volcano, Aegean island arc, Greece. J Volcanol Geoth Res 46:231–240
Sodoudi F, Kind R, Hatzfeld D, Priestley K, Hanka W, Wylegalla K et al (2006) Lithospheric structure of the Aegean obtained from P and S receiver functions. J Geophys Res 111:B12307
Sotiropoulos S, Kamperls E, Triantaphyllou M (2003) Thrust sequences in the central part of the external hellenides. Geol Mag 140(6):661–668
Spandler C, Mavrogenes J, Hermann J (2007) Experimental constraints on element mobility from subducted sediments using high-P synthetic fluid/melt inclusions. Chem Geol 239:228–249
Spencer KJ, Lindsley DH (1981) A solution model for coexisting iron-titanium oxides. Am Miner 66(11–12):1189–1201
Stouraiti C, Mitropoulos P, Tarney J, Barreiro B, McGrath AM, Baltatzis E (2010) Geochemistry and petrogenesis of late Miocene granitoids, Cyclades, southern Aegean: nature of source components. Lithos 114:337–352
Stouraiti C, Pantziris I, Vasilatos C, Kanellopoulos C, Mitropoulos P, Pomonis P et al (2017) Ophiolitic remnants from the upper and intermediate structural unit of the Attic-Cycladic Crystalline Belt (Aegean, Greece): fingerprinting geochemical affinities of magmatic precursors. Geosciences 7(1):14
Stracke A, Zindler A, Salters VJ, McKenzie D, Blichert-Toft J, Albarède F, Grönvold K (2003) Theistareykir revisited. Geochem Geophys Geosyst 4(2):8507
Straub SM, LaGatta AB, Martin-Del Pozzo AL, Langmuir CH (2008) Evidence from high-Ni olivines for a hybridized peridotite/pyroxenite source for orogenic andesites from the central Mexican Volcanic Belt. Geochem Geophys Geosyst 9(3):Q03007
Sun SS, McDonough WF (1989) Chemical and isotopic systematics of oceanic basalts: implications for mantle composition and processes. In: Saunders AD, Norry MJ (eds.), Magmatism in the ocean basins, Geol Soc London, Special Publications 42:313–345
Sun CH, Stern RJ (2001) Genesis of Mariana shoshonites: contribution of the subduction component. J Geophys Res 106:589–608
Taymaz T, Yilmaz Y, Dilek Y (2007) The geodynamics of the Aegean and Anatolia. Geol Soc Lond Spec Publ 291:1–16
Thirlwall MF, Upton BG, Jenkins C (1994) Interaction between continental lithosphere and the Iceland plume: Sr-Nd-Pb isotope geochemistry of tertiary basalts. NE Greenland J Petrol 35(3):839–879
Thomson SN, Ring U, Brichau S, Glodny J, Thomas M (2009) Timing and nature of formation of the Ios metamorphic core complex, southern Cyclades, Greece. Geol Soc Lond Spec Publ 321:139–167
Tiepolo M, Vannucci R, Bottazzi P, Oberti R (2000) Partitioning of rare earth elements, Y, Th, U, and Pb between pargasite, kaersutite, and basanite to trachyte melts: Implications for percolated and veined mantle. Geochem Geophys Geosyst 1:8
Tirel C, Gueydan F, Tiberi C, Brun JP (2004) Aegean crustal thickness inferred from gravity inversion. Geodyn Implic Earth Planet Sci Lett 228(3–4):267–280
Tranos M (2009) Faulting of Lemnos Island; a mirror of faulting of the North Aegean Trough (Northern Greece). Tectonophysics 467(1–4):72–88
van Hinsbergen DJ, Langereis CG, Meulenkamp JE (2005) Revision of the timing, magnitude and distribution of Neogene rotations in the western Aegean region. Tectonophysics 396(1–2):1–34
Vlahou M, Christofides G, Eleftheriadis G, Pinarelli L, Koroneos A (2006) Tertiary volcanic rocks from Samothraki island (north Aegean, Greece): Sr and Nd isotope constraints on their evolution. Geol Soc Am, Special Papers 409:283–304
Waters LE, Lange RA (2015) An updated calibration of the plagioclase-liquid hygrometer-thermometer applicable to basalts through rhyolites. A Miner 100:2172–2184
Wen G, Li JW, Hofstra AH, Koenig AE, Lowers HA, Adams D (2017) Hydrothermal reequilibration of igneous magnetite in altered granitic plutons and its implications for magnetite classification schemes: Insights from the Handan-Xingtai iron district, North China Craton. Geochim Cosmochim Acta 213:255–270
Wheller GE, Varne R, Foden JD, Abbott MJ (1987) Geochemistry of quaternary volcanics in the Sunda-Banda arc, Indonesia, and three-component genesis of island-arc basaltic magmas. J Volcanol Geoth Res 32(1–3):137–160
Workman R, Hart S (2005) Major and trace element composition of the depleted MORB mantle (DMM). Earth Planet Sci Lett 23:53–72